Journal of Applied Mathematics

WILEY

RESEARCH ARTICLE OPEN ACCESS

Complex Dynamics of a Predator–Prey System With Fear Effect in Prey

Anal Chatterjee[1] | Muhammad Aqib Abbasi[2] | Stacey R. Smith?[3] | Mainul Haque[4]

[1]Department of Mathematics, Barrackpore Rastraguru Surendranath College, Kolkata, India | [2]Department of Mathematics, Quaid-I-Azam University, Islamabad, Pakistan | [3]Department of Mathematics, The University of Ottawa, Ottawa, Ontario, Canada | [4]Department of Mathematical Sciences, University of Nottingham Ningbo China, Ningbo, China

Correspondence: Mainul Haque (mainul.haque@nottingham.edu.cn)

Received: 4 July 2025 | **Revised:** 27 January 2026 | **Accepted:** 3 March 2026

Academic Editor: Soufiane Bentout

Keywords: chaotic dynamics | global sensitivity analysis | Lyapunov coefficients | Lyapunov exponent | mathematical ecology | multivariable calculus

ABSTRACT

This study investigates the dynamical consequences of predator-induced fear in a predator–prey system by integrating nonlinear fear effects, intraspecific competition, and Holling type II predation. We analyze both continuous- and discrete-time formulations to capture a wide spectrum of ecological dynamics. The model exhibits rich behaviors, including stable coexistence, bistability, oscillations, and chaotic dynamics, revealing how fear can fundamentally reshape population interactions. Analytical results establish well-posedness and persistence, while numerical bifurcation analysis demonstrates that variations in key ecological parameters can trigger qualitative transitions such as oscillatory outbreaks and complex irregular fluctuations. Global sensitivity analysis identifies the dominant parameters controlling long-term population densities, thereby quantifying system robustness. To account for environmental variability, a stochastic extension with multiplicative noise is examined, showing that moderate fluctuations preserve coexistence, whereas strong disturbances may destabilize populations. Discrete-time analysis further uncovers period-doubling routes to chaos and intricate bifurcation structures. Overall, the results highlight predator-induced fear as a critical regulatory mechanism that can either stabilize or destabilize ecosystems, offering important ecological insights into population management and the prediction of complex biological dynamics.

JCL Classification: 92D40; 92D25

1 | Introduction

Predator–prey interactions constitute a fundamental component of ecological systems and have long served as a cornerstone of research in both theoretical ecology and mathematical biology. Understanding how predators regulate prey populations is a central ecological question. Traditional predator–prey formulations, particularly those derived from the Lotka–Volterra framework, typically regard direct predation as the principal mechanism influencing prey density [1–5]. While direct killing is readily observable in nature, growing empirical evidence suggests that predators can influence prey populations through additional, indirect pathways.

One such pathway is predator-induced fear, which can substantially modify prey behavior and physiology. The mere presence of predators may cause prey to alter habitat use, reduce foraging activity, increase vigilance, or undergo stress-related physiological changes [6–9]. Although these antipredator strategies may enhance short-term survival, they often incur energetic costs that suppress growth and reproduction. Consequently, fear effects can reduce prey fitness and population size, sometimes exerting a stronger influence than direct predation itself.

The role of fear-induced behavioral responses has been widely examined in predator–prey systems through deterministic

modeling frameworks. Fear is typically incorporated as a parameter modifying prey reproduction or interaction terms, leading to significant qualitative changes in system dynamics. Sasmal et al. [10] reported multistability in a model with group defense and a Holling type IV functional response. Panday et al. [11] showed that fear can suppress chaos via period-halving bifurcations in a tritrophic system. Incorporating reproductive costs of fear, Sarkar and Khajanchi [12] demonstrated stabilization through the removal of persistent oscillations. The interplay between fear and supplementary resources was investigated by Mondal et al. [13], while Wang and Zou [9] analyzed delay-induced stability switches. These results confirm that fear functions as a critical bifurcation parameter influencing equilibrium stability and long-term dynamical behavior.

Beyond its influence on reproduction, predator-induced fear can also affect prey mortality. Predator encounters do not always result in immediate capture; injured prey may escape initially but die later due to wounds or physiological stress [14]. Moreover, chronic exposure to predation risk can elevate stress hormone levels and deplete energy reserves, further increasing mortality risk [15, 16]. Despite this, many existing models consider fear effects only through reduced prey reproduction, overlooking their potential contribution to prey death rates.

In addition to fear effects, realistic predator–prey modeling requires accounting for intraspecific competition within predator populations. When predator density becomes high relative to prey availability, competition for limited resources reduces individual fitness and survival [17]. Such competition has been observed in various ecological contexts, including blue-crab populations, where aggressive interactions and injuries become more frequent under food scarcity [18]. Incorporating predator self-regulation through intraspecific competition has been shown to significantly alter system stability and long-term dynamics [5, 19].

Another important limitation of deterministic predator–prey models is their inability to capture environmental variability. Natural ecosystems are subject to random fluctuations arising from climate variability, resource availability, and other unpredictable factors. Stochastic formulations, especially those driven by Gaussian white noise, offer a more appropriate description of rapid environmental variability [20, 21]. White noise perturbations modeled via Wiener processes have been successfully applied to ecological systems to assess the robustness of dynamic behaviors under uncertainty [22, 23]. However, to the best of our knowledge, predator–prey models simultaneously incorporating fear effects, predator interference, and stochastic environmental fluctuations remain largely unexplored.

Recently, the concept of fear ecology has also been extended to marine ecosystems, particularly plankton-based food webs. Several studies have investigated how fear influences interactions among phytoplankton, zooplankton, and higher trophic levels, revealing its potential role in shaping marine population dynamics [24–26]. These findings further underscore the broad ecological relevance of fear-mediated interactions across both terrestrial and aquatic systems.

Unlike these diffusion-driven and harvesting-based models, the present study emphasizes the nonlinear effects of predator-induced fear on prey growth and ecosystem stability. Using Lyapunov exponents and bifurcation theory, we reveal complex oscillatory and chaotic behaviors emerging from fear dynamics—an aspect yet to be addressed in the existing literature.

This work investigates the joint impact of bottom-up resource regulation and top-down predation pressure within a predator–prey framework. We incorporate a fear-mediated modification in the predators' intraspecific competition and adopt a Holling type II functional response to characterize predation dynamics. The inclusion of the functional response ensures a realistic representation of consumption rates and saturation effects, thereby preserving the biological consistency of the system.

The goal of this research is to address the following biological questions.

- Can the fear level of prey increase the stability of the predator–prey system?
- How do the dynamics of the predator–prey system change in response to variations in the predator population's consumer rate and mortality rate?
- What role does predator conversion efficiency play in regulating the dynamic behavior of the predator–prey system?

The paper is organized as follows. The construction of a mathematical model based on the above set of assumptions is performed in Section 2. In Section 3, the well-posedness of the model and the boundedness of solutions are established. Section 4 is devoted to a detailed analytical investigation of the system dynamics, including the existence of equilibria, their local stability properties, and the associated bifurcation analysis. Comparative studies of two systems are summarized in Section 5. The next section is devoted to the global sensitivity analysis of the model. The coexistence equilibrium point's stochastic stability is addressed in Section 7. Sections 8 and 9, respectively, contain the numerical simulations of continuous and discrete system. Finally, Section 10 concludes the paper with a summary of the main results, ecological interpretations, and directions for future research.

2 | The Mathematical Model

This section develops the mathematical formulation of the system by incorporating interspecies competition [5, 19] in the predator and prey fear [7, 27], and our model takes the form

$$\left.\begin{aligned}\frac{dx}{dt} &= \frac{rx}{Ky+1} - r_1x^2 - \frac{mxy}{ax+b} \coloneqq f_1(x,y)\\ \frac{dy}{dt} &= \frac{emxy}{ax+b} - dy - hy^2 \coloneqq f_2(x,y)\end{aligned}\right\}. \tag{1}$$

System (1) is analyzed with the following initial conditions:

$$\begin{aligned}x(0) &\geq 0,\\ y(0) &\geq 0.\end{aligned} \tag{2}$$

The model describes a predator–prey system in which $x(t)$ and $y(t)$ represent the population densities of the prey and predator, respectively, at time t.

In this formulation, the symbols have the following biological meanings:

- r is the prey's intrinsic growth rate,
- r_1 measures the reduction in prey growth due to intraspecific competition,
- m characterizes the rate at which an individual predator consumes prey,
- e denotes the conversion efficiency of prey biomass into predator growth,
- a denotes the predator's attack rate on prey,
- b is the handling time (the time a predator spends processing each prey),
- d is the predator's natural death rate,
- h quantifies intraspecific competition among predators, and
- K represents the level of prey fear caused by antipredator reactions.

A prey-dependent predator–prey model is formulated incorporating the following features:

- A Holling type II functional response.
- The prey grows logistically.
- The prey population exhibits fear-driven antipredator behavior [7].

Using K to represent the level of prey fear caused by antipredator reactions, we can express it explicitly as

$$F(y; K) = \frac{r}{1 + Ky}. \tag{3}$$

Here, $F(y; K)$ denotes the effective reproduction rate of the prey population under the influence of fear, while K quantifies the level of prey fear caused by antipredator responses. Biologically, an increase in K reflects stronger fear effects (e.g., reduced foraging or reproduction due to predator presence), which leads to a decline in the prey's reproductive rate.

Ecological considerations motivate the following assumptions on $(y; K)$:

1. $F(y; 0) = r$: the reproduction rate of the prey remains constant without the fear effect.
2. $F(0; K) = r$: the prey's reproductive rate remains consistent in the absence of the predator.
3. $\lim_{K \longrightarrow \infty} F(y; K) = 0$: fearful prey under strong fear pressure cannot reproduce.
4. $\lim_{y \longrightarrow \infty} F(y; K) = 0$: reproduction among prey becomes impossible when predator density becomes sufficiently large.
5. With a high level of fear, the prey reproduction rate decreases

$$\frac{\partial F(y; K)}{\partial K} < 0. \tag{4}$$

6. With a high predator density, the prey reproduction rate decreases

$$\frac{\partial F(y; K)}{\partial y} < 0. \tag{5}$$

3 | Some Preliminary Results

3.1 | Positivity and Boundedness of Solutions

The validity of the model relies on demonstrating the positivity and boundedness of solutions for System (1). We prioritize establishing the positivity of the solutions, highlighting their significance.

Proposition 1. *For each initial condition $(x_0, y_0) \in \mathbb{R}^2_+$, System (1) admits a unique solution $(x(t), y(t))$ such that $x(t) > 0$ and $y(t) > 0$ for all $t > 0$.*

Proof 1. See Appendix A1 □

3.2 | Boundedness of the System

Proposition 2. *The region*

$$\triangle = \left\{(x, y) \in \mathbb{R}^2_+ \colon 0 \le x + \frac{1}{e} y \le \frac{\widehat{M}}{\gamma}\right\} \tag{6}$$

contains all solutions of System (1) as $t \longrightarrow \infty$ for all positive initial values $(x_0, y_0) \in \mathbb{R}^2_+$, where $\gamma < \min\{r, d\}$ and $\widehat{M} = r^2/r_1$.

Proof 2. See Appendix A2. □

3.3 | Persistence

The non-negativity of solutions to System (1) is a necessary property for biological validity and long-term population sustainability. For persistence of System (1), there exists a compact set $D_1 \subset \Psi_1 = \{(x, y) \colon x > 0, \quad y > 0\}$ such that every solution ultimately enters D_1 and remains there for all sufficiently large t.

Proposition 3. *System (1) exhibits persistence if the following conditions are satisfied:*

$$r > d, \tag{7}$$

$$m > \frac{1}{e}\left[\frac{bdr_1}{r} + da\right]. \tag{8}$$

Proof 3. See Appendix A3. □

4 | Stability and Bifurcation Analyses of the Model (1)

This section presents a comprehensive analytical study of the system dynamics, focusing on equilibrium analysis, local stability properties, and bifurcation behavior with respect to key model parameters.

The steady states of System (1) are obtained by solving the nonlinear algebraic equations $f_1(x, y) = 0$ and $f_2(x, y) = 0$. We denote the equilibria by $E_0(0, 0)$, $E_1(r/r_1, 0)$, and $E^*(x^*, y^*)$, corresponding to the extinction state, the predator-free state, and the interior coexistence state, respectively.

To investigate local stability, we linearize System (1) around an arbitrary equilibrium point. This is accomplished by evaluating

the associated Jacobian matrix at each steady state, which determines the qualitative behavior of solutions in its neighborhood.

The Jacobian matrix at $\overline{E} = (\overline{x}, \overline{y})$ is given by

$$\overline{J} = \begin{pmatrix} \dfrac{r}{K\overline{y}+1} + \dfrac{am\overline{x}\overline{y}}{(b+a\overline{x})^2} - 2\overline{x}r_1 - \dfrac{m\overline{y}}{b+a\overline{x}} & -\dfrac{m\overline{x}}{b+a\overline{x}} - \dfrac{Kr\overline{x}}{(K\overline{y}+1)^2} \\ \dfrac{em\overline{y}}{b+a\overline{x}} - \dfrac{aem\overline{x}\overline{y}}{(b+a\overline{x})^2} & -d - 2h\overline{y} + \dfrac{em\overline{x}}{b+a\overline{x}} \end{pmatrix}. \tag{9}$$

4.1 | Existence and Stability of Trivial and Predator-Free Equilibria

This subsection analyzes the system's local behavior (1) around its trivial and predator-free equilibrium points.

4.1.1 | Trivial Equilibrium $E_0(0, 0)$

The trivial equilibrium $E_0(0, 0)$ exists for all admissible parameter values. Substituting this point into the Jacobian matrix (9) gives the eigenvalues $-d < 0$ and $r > 0$. Since one eigenvalue is positive and the other is negative, E_0 is a saddle point and therefore unstable.

4.1.2 | Predator-Free Equilibrium E_1

The boundary equilibrium E_1 is characterized by $x_1 = r/r_1$ and $y_1 = 0$. Linearization of System (9) about E_1 yields two real eigenvalues,$-r < 0$ and $\mu_2(R_0 - 1)$. The threshold quantity R_0 is defined by

$$R_0 = \frac{emr}{d(br_1 + ar)} < 1. \tag{10}$$

Consequently, E_1 attains local asymptotic stability precisely when Condition (10) holds.

4.2 | Existence and Stability of the Coexistence Equilibrium $E^* = (x^*, y^*)$

This subsection analyzes the system's local behavior (1) around its coexistence equilibrium point. The interior equilibrium $E^* = (x^*, y^*)$ does not admit a closed-form expression. In particular, y^* can be written in terms of x^* as $y^* = (1/h)((emx^*)/(ax^* + b) - d)$. Substituting this expression into the equilibrium condition leads to a quartic polynomial equation in x^* which is represented by

$$\sum_{n=0}^{4} B_n X^n = 0, \tag{11}$$

whose coefficients are

$$\begin{aligned} B_4 &= \left(-a^3h^2r_1 + a^3dhKr_1 - a^2ehKmr_1\right), \\ B_3 &= \left(a^3h^2r - 3a^2bh^2r_1 + 3a^2bdhKr_1 - 2abehKmr_1\right), \\ B_2 &= \left(a^2dhm - a^2d^2Km - aehm^2 + 2adeKm^2 - e^2Km^3 + 3a^2bh^2r - 3ab^2h^2r_1 + 3ab^2dhKr_1 - b^2ehKmr_1\right), \\ B_1 &= \left(2abdhm - 2abd^2Km - behm^2 + 2bdeKm^2 + 3ab^2h^2r - b^3h^2r_1 + b^3dhKr_1\right), \\ B_0 &= b^2dhm - b^2d^2Km + b^3h^2r. \end{aligned} \tag{12}$$

Next, we analyze the corresponding algebraic equation and derive parameter conditions under which its roots remain positive. Figure 1 illustrates the prey and predator nullclines of the system, whose relative positions and intersection explain the existence and local stability of the coexistence equilibrium E^*, thereby providing a geometric interpretation of the underlying dynamics.

To establish the coexistence equilibrium, we require at least one positive root of (11). In general, this polynomial can possess up to four complex zeros. We assume that two of them form a conjugate pair, denoted by $\widehat{\alpha}$ and $\widehat{\alpha^*}$. Accordingly, the associated quadratic factor takes the following form [28]:

$$X^2 + \widehat{\theta}_1 X + \widehat{\theta}_2 = (X - \widehat{\alpha})\left(X - \widehat{\alpha^*}\right) = X^2 - 2\mathrm{Re}\,(\widehat{\alpha})X + |\widehat{\alpha}|^2, \tag{13}$$

where $\widehat{\theta}_1 = -2\mathrm{Re}(\widehat{\alpha})$ and $\widehat{\theta}_2 = |\widehat{\alpha}|^2$.

We suppose that Equation (11) possesses two real solutions x_1^* and x_2^*, satisfying $(x_1^* + x_2^*) = -\widehat{p}_r$ and $x_1^* x_2^* = \widehat{q}_s$.

As a result, the factorization of equation (11) can be expressed as follows:

$$\begin{aligned} \sum_{n=0}^{4} B_n X^n &= B_4\left(X^2 + \widehat{\theta}_1 X + \widehat{\theta}_2\right)\left(X^2 + \widehat{p}_r X + \widehat{q}_s\right) \\ &= B_4\left[X^4 + \left(\widehat{p}_r + \widehat{\theta}_1\right)X^3 + \left(\widehat{\theta}_2 + \widehat{q}_s + \widehat{\theta}_1\widehat{p}_r\right)X^2 + \left(\widehat{\theta}_1\widehat{q}_s + \widehat{\theta}_2\widehat{p}_r\right)X + \widehat{\theta}_2\widehat{q}_s\right]. \end{aligned} \tag{14}$$

Equating coefficients in the factorized expression yields

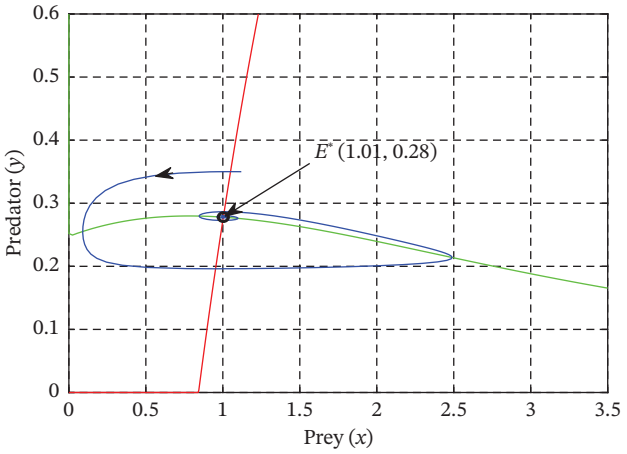

FIGURE 1 | The prey–predator nullcline configuration (green for prey and red for predator) corresponding to the parameter set (56) is presented together with a numerical trajectory generated in MATLAB using a step size $\Delta t = 0.01$ and initial condition $(1.12, 0.35)$ illustrating convergence toward the equilibrium E^*.

$$\begin{aligned}\widehat{p}_r &= \frac{B_3}{B_4} + 2\mathrm{Re}(\widehat{\alpha}),\\ \widehat{q}_s &= \frac{B_0}{B_4|\widehat{\alpha}|^2}.\end{aligned} \tag{15}$$

We next analyze the two admissible cases.

Case 1: Suppose that $\widehat{q}_s > 0$ and $\widehat{p}_r < 0$. In particular, when $(ah)/(ad - em) < K < (dhm + bh^2r)/(d^2m)$, the quadratic equation admits two distinct real roots. Moreover, both roots are positive provided that the discriminant condition $\widehat{p}_r^2 - 4\widehat{q}_s > 0$ holds.

Therefore, the two distinct positive real roots are obtained as follows:

$$\begin{aligned}x_1^* &= \frac{-\widehat{p}_r + \sqrt{\widehat{p}_r^2 - 4\widehat{q}_s}}{2},\\ x_2^* &= \frac{-\widehat{p}_r - \sqrt{\widehat{p}_r^2 - 4\widehat{q}_s}}{2}.\end{aligned} \tag{16}$$

The admissibility of these roots requires $B_3 < 0$ together with $\widehat{p}_r^2 - 4\widehat{q}_s > 0$.

Case 2: Suppose that $\widehat{q}_s < 0$, which arises whenever $\mathrm{Max}\{(dhm + bh^2r)/(d^2m), (ah)/(ad - em)\} < K$. In this situation, the quadratic equation admits exactly one positive real root consistent with the stated requirements. Consequently, the coexistence equilibrium $E^*(x^*, y^*)$ exists whenever the above conditions are fulfilled.

$$\begin{aligned}&(a)\colon x^* > \frac{bd}{em - ad},\ (b)\colon m > \frac{ad}{e},\\ &(c)\colon \widehat{p}_r^2 - 4\widehat{q}_s > 0,\ (d)\colon \mathrm{Max}\left\{\frac{\mathrm{dhm} + bh^2r}{d_2m}, \frac{ah}{ad - em}\right\} < K.\end{aligned} \tag{17}$$

Thus, $E^*(x^*, y^*)$ exists whenever $x^* > 0$ and $y^* > 0$.

$$J^* = \begin{pmatrix} \dfrac{amx^*y^*}{(ax^* + b)^2} - r_1x^* & -x^*\left(\dfrac{m}{ax^* + b} + \dfrac{Kr}{(Ky^* + 1)^2}\right)\\ \dfrac{bemy^*}{(ax^* + b)^2} & -hy^* \end{pmatrix}. \tag{18}$$

The linearization of the system at the coexistence equilibrium E^* yields the characteristic polynomial

$$\lambda^2 + Q_1\lambda + Q_2 = 0, \tag{19}$$

where

$$\begin{aligned}Q_1 &= x^*\left(r_1 - \frac{may^*}{(ax^* + b)^2}\right) + hy^*,\\ Q_2 &= hx^*y^*\left(r_1 - \frac{may^*}{(ax^* + b)^2}\right) + \frac{bemx^*y^*}{(ax^* + b)^2}\left(\frac{m}{ax^* + b} + \frac{Kr}{(Ky^* + 1)^2}\right).\end{aligned} \tag{20}$$

Now, $Q_1 > 0$, and $Q_2 > 0$ if

$$r_1 > \frac{may^*}{(ax^* + b)^2}. \tag{21}$$

In this case, Equation (19) has two roots with negative real parts, indicating that the local stability of E^* is evident.

Thus, violation of condition (21) may lead to the occurrence of the "paradox of enrichment" in System (1).

4.3 | Global Stability at E^*

Building on the local stability results, this subsection examines the global stability of the coexistence equilibrium E^* using Lyapunov methods.

Proposition 4. *If $r_1 > (amy^*)/(ax^* + b)$, then E^* is globally asymptotically stable.*

Proof 4. See Appendix A4. □

4.4 | Hopf Bifurcation at $E^* = (x^*, y^*)$

This subsection investigates the Hopf bifurcation of System (1) around the coexistence equilibrium E^*, identifying the critical parameter values at which periodic oscillations emerge.

Proposition 5. *The necessary and sufficient conditions for Hopf bifurcation of (1) at E^* for $m = m^H$ are*

$$[tr(J^*)]_{m=m^H} = 0, [\det(J^*)]_{m=m^H} > 0, \text{and } \frac{d}{dm}[tr(J^*)]_{m=m^H} \neq 0. \tag{22}$$

Proof 5. See Appendix A5. □

4.4.1 | Direction of Hopf Bifurcation at $E^* = (x^*, y^*)$

Taking m as the bifurcation parameter, the preceding result establishes that System (1) exhibits a Hopf bifurcation at the coexistence equilibrium $E^*(x^*, y^*)$. We now investigate the direction of the bifurcation and the stability of the periodic solutions emanating from E^*. For this purpose, the first Lyapunov coefficient is evaluated, and the criteria stated in [29] are

employed. To facilitate the analysis, the equilibrium $E^*(x^*, y^*)$ is shifted to the origin via the transformation $\hat{z}_1 = x - x^*$, $\hat{z}_2 = y - y^*$. In terms of the new variables, system (1) takes the form

$$\frac{d\hat{z}_1}{dt} = \frac{r(\hat{z}_1 + x^*)}{1 + K(\hat{z}_2 + y^*)} - r_1(\hat{z}_1 + x^*)^2 - \frac{m(\hat{z}_1 + x^*)(\hat{z}_2 + y^*)}{a_1(\hat{z}_1 + x^*) + b}, \tag{23}$$

$$\frac{d\hat{z}_2}{dt} = \frac{em(\hat{z}_1 + x^*)(\hat{z}_2 + y^*)}{a(\hat{z}_1 + x^*) + b} - d(\hat{z}_2 + y^*) - h(\hat{z}_2 + y^*)^2. \tag{24}$$

Truncating the Taylor series at third order about $(\hat{z}_1, \hat{z}_2) = (0, 0)$ yields the following dynamical system:

$$\begin{aligned}
\dot{\hat{z}}_1 &= \bar{c}_{10}\hat{z}_1 + \bar{c}_{01}\hat{z}_2 + \bar{c}_{20}\hat{z}_1^2 + \bar{c}_{11}\hat{z}_1\hat{z}_2 + \bar{c}_{02}\hat{z}_2^2 + \bar{c}_{30}\hat{z}_1^3 + \bar{c}_{21}\hat{z}_1^2\hat{z}_2 + \bar{c}_{12}\hat{z}_1\hat{z}_2^2 + \bar{c}_{03}\hat{z}_2^3 + \mathcal{O}(|\hat{z}|^4),\\
\dot{\hat{z}}_2 &= \bar{d}_{10}\hat{z}_1 + \bar{d}_{01}\hat{z}_2 + \bar{d}_{20}\hat{z}_1^2 + \bar{d}_{11}\hat{z}_1\hat{z}_2 + \bar{d}_{02}\hat{z}_2^2 + \bar{d}_{30}\hat{z}_1^3 + \bar{d}_{21}\hat{z}_1^2\hat{z}_2 + \bar{d}_{12}\hat{z}_1\hat{z}_2^2 + \bar{d}_{03}\hat{z}_2^3 + \mathcal{O}(|\hat{z}|^4),
\end{aligned} \tag{25}$$

where

$$\begin{aligned}
&\bar{c}_{10} = -r_1x^* + \frac{\mathrm{amx}^*y^*}{(ax^* + b)^2}, \bar{c}_{01} = -x^*\left\{\frac{m}{ax^* + b} + \frac{Kr}{(1 + Ky^*)^2}\right\}, \bar{c}_{20} = -\left\{r_1 - \frac{\mathrm{abmy}^*}{(ax^* + b)^3}\right\},\\
&\bar{c}_{11} = -\left\{\frac{bm}{(ax^* + b)^2} + \frac{Kr}{(1 + Ky^*)^2}\right\}, \bar{c}_{02} = \frac{rK^2x^*}{(1 + Ky^*)^2}, \bar{c}_{30} = -\frac{a^2bmy^*}{(ax^* + b)^4},\\
&\bar{c}_{21} = \frac{\mathrm{abm}}{(ax^* + b)^3}, \bar{c}_{12} = \frac{rK^2}{(1 + Ky^*)^3}, \bar{c}_{03} = -\frac{rK_3x^*}{(1 + Ky^*)^4},\\
&\bar{d}_{10} = \frac{\mathrm{bemy}^*}{(ax^* + b)^2}, \bar{d}_{01} = -hy^*, \bar{d}_{20} = -\frac{\mathrm{abemy}^*}{(ax^* + b)^3}, \bar{d}_{11} = \frac{\mathrm{bem}}{(ax^* + b)^2}, \bar{d}_{02} = -h,\\
&\bar{d}_{30} = \frac{a^2\mathrm{bemy}^*}{(ax^* + b)^4}, \bar{d}_{21} = -\frac{\mathrm{abem}}{(ax^* + b)^3}, \bar{d}_{12} = 0, \bar{d}_{03} = 0.
\end{aligned} \tag{26}$$

Neglecting the higher-order terms, we reformulate system (25) as follows:

$$\dot{\hat{Z}} = J_E^*\hat{Z} + \hat{H}(\hat{Z}), \quad \hat{Z} = \begin{pmatrix}\hat{z}_1,\\ \hat{z}_2.\end{pmatrix}, \tag{27}$$

where

$$\begin{aligned}
\hat{H} &= \begin{pmatrix}\hat{H}_1\\ \hat{H}_2\end{pmatrix}\\
&= \begin{pmatrix}\bar{c}_{20}\hat{z}_1^2 + \bar{c}_{11}\hat{z}_1\hat{z}_2 + \bar{c}_{02}\hat{z}_2^2 + \bar{c}_{30}\hat{z}_1^3 + \bar{c}_{21}\hat{z}_1^2\hat{z}_2 + \bar{c}_{12}\hat{z}_1\hat{z}_2^2 + \bar{c}_{03}\hat{z}_2^3\\ \bar{d}_{20}\hat{z}_1^2 + \bar{d}_{11}\hat{z}_1\hat{z}_2 + \bar{d}_{02}\hat{z}_2^2 + \bar{d}_{30}\hat{z}_1^3 + \bar{d}_{21}\hat{z}_1^2\hat{z}_2 + \bar{d}_{12}\hat{z}_1\hat{z}_2^2 + \bar{d}_{03}\hat{z}_2^3\end{pmatrix}.
\end{aligned} \tag{28}$$

At $m = m_1^H$, the eigenvector $\hat{v}$ of the Jacobian matrix J_E^* corresponding to the eigenvalues $i\omega_0$ is given by $\hat{v} = (\bar{c}_{01}, i\omega_0 - \bar{c}_{10})^T$. Now, let us define

$$S = (\mathrm{Re}(\hat{v}), -\mathrm{Im}(\hat{v})) = \begin{pmatrix}\bar{c}_{01} & 0\\ -\bar{c}_{10} & -\omega_0\end{pmatrix}. \tag{29}$$

Let $\hat{Z} = SY$ or $Y = S^{-1}\hat{Z}$, where $Y = (y_1, y_2)^T$. Under the above transformation, system (27) can be expressed in the form $\dot{Y} = (S^{-1}J_E^*S)Y + S^{-1}\hat{H}(SY)$. Equivalently, it reduces to

$$\begin{pmatrix}\dot{y}_1\\ \dot{y}_2\end{pmatrix} = \begin{pmatrix}0 & -\omega_0\\ \omega_0 & 0\end{pmatrix}\begin{pmatrix}y_1\\ y_2\end{pmatrix} + \begin{pmatrix}\hat{Q}^1(y_1, y_2; m = m^H)\\ \hat{Q}^2(y_1, y_2; m = m^H)\end{pmatrix}, \tag{30}$$

where $\hat{Q}^1$ and $\hat{Q}^2$ denote the higher-order nonlinear terms in y_1 and y_2. In particular, these functions are given by

$$\begin{aligned}
\hat{Q}^1(y_1, y_2; m_1 = m^H) &= \frac{1}{\bar{c}_{01}}\hat{H}_1, \hat{Q}^2(y_1, y_2; m_1 = m^H)\\
&= -\frac{1}{\omega_0\bar{c}_{01}}\left(\bar{c}_{10}\hat{H}_1 + \bar{c}_{01}\hat{H}_2\right),
\end{aligned} \tag{31}$$

with

$$\begin{aligned}\widehat{H}_1 = &\left(\bar{c}_{20}\bar{c}_{01}^2 - \bar{c}_{11}\bar{c}_{01}\bar{c}_{10} + \bar{c}_{02}\bar{c}_{10}^2\right)y_1^2 + \omega_0\left(2\bar{c}_{02}\bar{c}_{10} - \bar{c}_{11}\bar{c}_{01}\right)y_1y_2 + \omega_0^2\bar{c}_{02}y_2^2\\ &+\left(\bar{c}_{12}\bar{c}_{01}\bar{c}_{10}^2 - \bar{c}_{03}\bar{c}_{10}^3 + \bar{c}_{30}\bar{c}_{01}^3 - \bar{c}_{21}\bar{c}_{01}^2\bar{c}_{10}\right)y_1^3 - \omega_0^3\bar{c}_{03}y_2^3 + \left(\omega_0 2\bar{c}_{12}\bar{c}_{10}\bar{c}_{01}\right.\\ &\left.-\bar{c}_{21}\bar{c}_{01}^2 - 3\bar{c}_{03}\bar{c}_{10}^2\right)y_1^2y_2 + \omega_0^2\left(\bar{c}_{12}\bar{c}_{01} - 3\bar{c}_{03}\bar{c}_{10}\right)y_1y_2^2,\end{aligned} \tag{32}$$

and

$$\begin{aligned}\widehat{H}_2 = &\left(\bar{d}_{20}\bar{c}_{01}^2 - \bar{d}_{11}\bar{c}_{01}\bar{c}_{10} + \bar{d}_{02}\bar{c}_{10}^2\right)y_1^2 + \omega_0\left(2\bar{d}_{02}\bar{c}_{10} - \bar{d}_{11}\bar{c}_{01}\right)y_1y_2 + \omega_0^2\bar{d}_{02}y_2^2\\ &+\left(\bar{d}_{12}\bar{c}_{01}\bar{c}_{10}^2 - \bar{d}_{03}\bar{c}_{10}^3 + \bar{d}_{30}\bar{c}_{01}^3 - \bar{d}_{21}\bar{c}_{01}^2\bar{c}_{10}\right)y_1^3 - \omega_0^3\bar{d}_{03}y_2^3 +\\ &\omega_0\left(2\bar{d}_{12}\bar{c}_{10}\bar{c}_{01} - \bar{d}_{21}\bar{c}_{01}^2 - 3\bar{d}_{03}\bar{c}_{10}^2\right)y_1^2y_2 + \omega_0^2\left(\bar{d}_{12}\bar{c}_{01} - 3\bar{d}_{03}\bar{c}_{10}\right)y_1y_2^2.\end{aligned} \tag{33}$$

To evaluate the stability and direction of a periodic solution, we compute the first Lyapunov coefficient [29]:

$$\begin{aligned}l_1 = &\frac{1}{16}\left[\widehat{Q}_{111}^1 + \widehat{Q}_{122}^1 + \widehat{Q}_{112}^2 + \widehat{Q}_{222}^2\right]\\ &+\frac{1}{16\omega_0}\left[\widehat{Q}_{12}^1\left(\widehat{Q}_{11}^1 + \widehat{Q}_{22}^1\right) - \widehat{Q}_{12}^2\left(\widehat{Q}_{11}^2 + \widehat{Q}_{22}^2\right) - \widehat{Q}_{11}^1\widehat{Q}_{11}^2 + \widehat{Q}_{22}^1\widehat{Q}_{22}^2\right],\end{aligned} \tag{34}$$

where

$$\begin{aligned}\widehat{Q}_{ij}^k &= \frac{\partial^2\widehat{Q}^k}{\partial y_i\partial y_j}|(y_1, y_2; m) = \left(0, 0; m^H\right),\\ \widehat{Q}_{ijl}^k &= \frac{\partial^3\widehat{Q}^k}{\partial y_i\partial y_j\partial y_l}|(y_1, y_2; m) = \left(0, 0; m^H\right), \quad i, j, k, l \in \{1, 2\}.\end{aligned} \tag{35}$$

The sign of the first Lyapunov coefficient determines the type of Hopf bifurcation: if $l_1 < 0$, it is a supercritical Hopf bifurcation, and if $l_1 > 0$, it is a subcritical Hopf bifurcation.

Remark 1. A straight forward calculation shows that $E_0(0, 0)$ is always unstable since one eigen value is $r > 0$ and $E_1(r/r_1, 0)$ is locally asymptotically stable iff $(emr)/(d(br_1 + ar)) < 1$. In addition, the trace and determinant of the Jacobian matrix of system (46) around $\widehat{E}^*(\hat{x}^*, \hat{y}^*)$ are $-\hat{x}^*(r_1 - (ma\hat{y}^*)/(a\hat{x}^* + b)^2) - h\hat{y}^*$, and $h\hat{x}^*\hat{y}^*(r_1 - (ma\hat{y}^*)/(a\hat{x}^* + b)^2) + ((bem\hat{x}^*\hat{y}^*)/(a\hat{x}^* + b)^2)(m/(a\hat{x}^* + b))$. For certain parameter values, the trace has the potential to become zero. This indicates the potential for obtaining purely imaginary roots, consequently leading to a Hopf bifurcation. The determinant has the potential to become zero within certain parametric ranges, leading to the emergence of bifurcations such as saddle-node bifurcations (SNB), transcritical bifurcations (TCBs), and Bogdanov–Takens bifurcation (BTB).

4.4.2 | A Normal Form of the BTB

We consider the planar system

$$\dot{\mathbf{x}} = f(\mathbf{x}, \breve{\mu}), \quad \mathbf{x} \in \mathbb{R}^2, \breve{\mu} \in \mathbb{R}^2, \tag{36}$$

where f is a smooth mapping. Suppose that $\mathbf{x} = 0$ is an equilibrium of (36) at $\breve{\mu} = 0$ and that the corresponding eigenvalues satisfy $\lambda_{1,2} = 0$. In addition, we assume that $J_{\mathbf{x}}f(0, 0)$ is nilpotent but not identically zero. Then, for $\breve{\mu} = 0$, System (36) can be expressed as

$$\dot{\mathbf{x}} = J_{\mathbf{x}}f(0, 0)\mathbf{x} + \mathbf{F}(\mathbf{x}), \tag{37}$$

where $\mathbf{F}(\mathbf{x}) = O(\|\mathbf{x}\|^2)$ contains all quadratic and higher order terms [30]. The matrix $J_{\mathbf{x}}f(0, 0)$ admits a single eigenvector $\breve{\mathbf{v}}_1$ corresponding to the double eigenvalue 0. In addition, there exists a generalized eigenvector $\breve{\mathbf{v}}_2$ such that

$$J_{\mathbf{x}}f(0, 0)\breve{\mathbf{v}}_2 = \breve{\mathbf{v}}_1. \tag{38}$$

Let $\breve{\mathbf{V}} = [\breve{\mathbf{v}}_1\breve{\mathbf{v}}_2]$ denote the nonsingular matrix formed by these linearly independent vectors. Introducing the coordinate transformation

$$\mathbf{y} = \breve{\mathbf{V}}^{-1}\mathbf{x}, \tag{39}$$

the system is converted into a C^∞-conjugate vector field given by

$$g = \breve{\mathbf{V}}^{-1} \circ f \circ \breve{\mathbf{V}}. \tag{40}$$

Specifically, when $\breve{\mu} = 0$, System (37) transforms into the following form:

$$\dot{\mathbf{y}} = \mathbf{J}_{\mathbf{y}}g(0, 0)\mathbf{y} + \left(\breve{\mathbf{V}}^{-1} \circ \mathbf{F} \circ \breve{\mathbf{V}}\right)(\mathbf{y}), \tag{41}$$

where

$$\mathbf{J}_{\mathbf{y}}g(0,0)=\begin{pmatrix}0 & 1\\ 0 & 0\end{pmatrix}. \tag{42}$$

Expanding (40) in a Taylor series with respect to $\mathbf{y}=(y_1,y_2)$ around $(y_1,y_2)=(0,0)$, we obtain the following expressions:

$$\begin{aligned}\dot{y_1}&=y_2+\check{a}_{00}(\check{\mu})+\check{a}_{10}(\check{\mu})y_1+\check{a}_{01}(\check{\mu})y_2+\frac{1}{2}\check{a}_{20}(\check{\mu})y_1^2+\check{a}_{11}(\check{\mu})y_1y_2+\frac{1}{2}\check{a}_{02}(\check{\mu})y_2^2+O(\|y\|^3),\\ \dot{y_2}&=\check{b}_{00}(\check{\mu})+\check{b}_{10}(\check{\mu})y_1+\check{b}_{01}(\check{\mu})y_2+\frac{1}{2}\check{b}_{20}(\check{\mu})y_1^2+\check{b}_{11}(\check{\mu})y_1y_2+\frac{1}{2}\check{b}_{02}(\check{\mu})y_2^2+O(\|y\|^3),\end{aligned} \tag{43}$$

where the coefficients $a_{ij}(\check{\mu})$ and $b_{ij}(\check{\mu})$ are smooth functions that can be determined from (36), (39), and (40). Specifically, at $\check{\mu}=0$, from (37) and (41), we find $\check{a}_{00}(0)=\check{a}_{10}(0)=\check{a}_{01}(0)=\check{b}_{00}(0)=\check{b}_{10}(0)=\check{b}_{01}(0)=0$. The following proposition characterizes the normal form of the BTB.

Proposition 6. *We consider the planar system (36) with $\check{\mu}=0$. Suppose that the origin is an equilibrium possessing a double zero eigenvalue; i.e., $\lambda_{1,2}(0)=0$. We assume the following genericity conditions:*

1. *The Jacobian $\mathbf{J}_{\mathbf{x}}f(0,0)$ is not the null matrix;*
2. *$\check{a}_{20}(0)+\check{b}_{11}(0)\neq 0$;*
3. *$\check{b}_{20}(0)\neq 0$;*
4. *The map $(\mathbf{x},\check{\mu})\mapsto(f(\mathbf{x},\check{\mu}),tr\mathbf{J}_{\mathbf{x}}f(\mathbf{x},\check{\mu}),\det\mathbf{J}_{\mathbf{x}}f(\mathbf{x},\check{\mu}))$ is regular at $(\mathbf{x},\check{\mu})=(0,0)\in\mathbb{R}^4$.*

Proof 6. Under these assumptions, one can introduce a smooth and locally invertible parameter transformation such that in a neighborhood of $(\mathbf{x},\check{\mu})=(0,0)$, the dynamics generated by f are topologically equivalent to the associated normal form

$$\left.\begin{aligned}\dot{\eta}_1&=\eta_2,\\ \dot{\eta}_2&=\alpha_1+\alpha_2\eta_2+\eta_2^2+s\eta_1\eta_2\end{aligned}\right\}, \tag{44}$$

where $s=\check{b}_{20}(0)(\check{a}_{20}(0)+\check{b}_{11}(0))=\pm 1$.

The normal form in (44) was first derived by Bogdanov [31], with an equivalent formulation independently obtained by Takens [32]. A comprehensive treatment and proof are provided in [33]. For brevity, the detailed computations establishing the presence of a BTB in System (1) are not included. Nevertheless, Conditions (1)–(4) ensure local topological equivalence to the corresponding normal form. Numerical simulations further corroborate the occurrence of the BTB (see Figures 2(a), 2(b), 2(c), and 2(d)).

Consequently, there exists a smooth local change of variables, together with an orientation-preserving time reparametrization and parameter transformation, under which System (1) is locally topologically conjugate, near $(x,y,m,b)=(0,0,m^*,b^*)$, to the Bogdanov–Takens normal form

$$\left.\begin{aligned}\dot{\eta}_1&=\eta_2,\\ \dot{\eta}_2&=\alpha_1+\alpha_2\eta_2+\eta_2^2\ \pm\ \eta_1\eta_2\end{aligned}\right\}, \tag{45}$$

where the sign of the nonlinear coupling term $\eta_1\eta_2$ is determined by $\check{a}_{20}(0)(\check{a}_{20}(0)+\check{b}_{11}(0))$. □

4.5 | TCB at E_1

This subsection is devoted to the analysis of a TCB of System (1) at the predator-free equilibrium point E_1.

Proposition 7. *As the system bifurcation parameter m surpasses the critical threshold $m=m^{TC}$, System (1) experiences a TCB.*

Proof 7. See Appendix A6. □

Figures 3(a) and 3(b) are intended to illustrate the qualitative change in system behavior occurring at the critical threshold $m=m^{TC}$. At this point, two equilibrium branches intersect and exchange their stability properties, which is the defining characteristic of a TCB. The graphical representation therefore provides a visual confirmation of the analytical results and clarifies how variations in the control parameter m drive transitions between different dynamical regimes of the model.

5 | Absence of Fear Effect

In this section, we compare the dynamics of System (1) in the presence and absence of the fear effect and summarize the findings in tabular form.

In absence of fear, System (1) takes the form:

$$\dot{Z}(t)=F(Z)=\left(\widehat{f}_1(Z)\widehat{f}_2(Z)\right)^T,\quad Z=(xy)^T\in\Omega_\delta, \tag{46}$$

where $\widehat{f}_1(Z)=rx-r_1x^2-(mxy)/(ax+b)$, $\widehat{f}_2(Z)=(emxy)/(ax+b)-dy-hy^2$, $\Omega_\delta=\{Z\in\mathbf{R}_+^2\}$, and $Z(0)\geq 0$. The initial findings, encompassing aspects such as solution existence, uniqueness, dissipativeness, and solution boundedness for System (46), can be readily demonstrated by employing the approaches outlined in Haque's work [19]. In a similar fashion, we checked the "permanence" and "paradox of enrichment" for the model (46) and summarized the results, in Tables 1 and 2, respectively, for comparison purposes with the Model (1).

Table 3 provides a comprehensive summary of the dynamics exhibited by Systems (1) and (46). In this context, LAS, GAS, and TCB represent local asymptotic stability, global asymptotic stability, and transcritical bifurcation.

6 | Global Sensitivity Analysis

A global sensitivity analysis of System (1) was conducted using Latin hypercube sampling (LHS) combined with partial rank correlation coefficients (PRCCs). LHS was applied to efficiently sample the parameter space, while PRCCs measured the

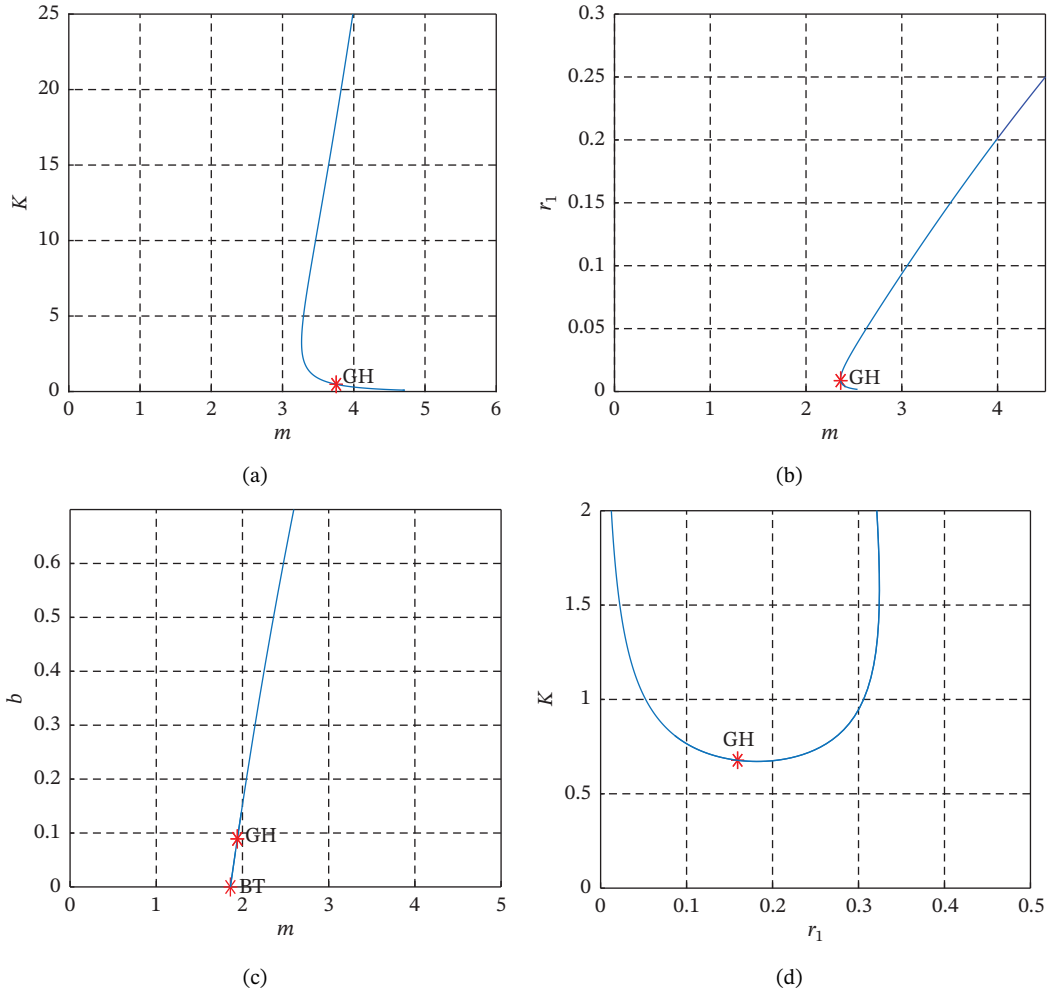

FIGURE 2 | (a–d) Bifurcation structures in the two-parameter planes (m, K), (m, r_1), (m, b), and (r_1, K), demonstrating the corresponding transitions in the qualitative behavior of the system.

monotonic influence of parameters on the prey population density.

A total of 5000 LHS realizations was generated, with each parameter independently sampled from a uniform distribution within ±50 % of its baseline value (see Equation (56)). Parameters with absolute PRCC values greater than ±0.5 were identified as having a strong impact on prey–predator dynamics. Accordingly, r, r_1, K, m, b, and d emerged as the most influential parameters, as illustrated in Figures 4(a) and 4(b).

7 | The Stochastic Model With White Noise

Deterministic predator–prey models assume constant environmental conditions, whereas real ecosystems are subject to random fluctuations caused by climate variability, resource availability, habitat disturbances, and disease. Such uncertainties can strongly influence population growth and species interactions and are not adequately described by deterministic dynamics alone. To capture these effects, we incorporate Gaussian white noise into the model, representing rapid and unpredictable environmental variations. Multiplicative noise is adopted since environmental disturbances typically scale with population density, ensuring that fluctuations weaken near equilibrium states and preserving biological realism. This stochastic formulation allows us to examine how environmental variability affects the stability of coexistence and to assess the resilience of predator–prey interactions under random perturbations, thereby providing a more realistic representation of population dynamics observed in nature.

This section investigates the influence of environmental variability on the proposed model. All parameters are assumed to be time-invariant, and particular attention is given to the stochastic stability of the coexistence equilibrium. A deterministic framework can account for environmental variability by treating key parameters as random or by superimposing stochastic effects on the evolution equations [34, 35]. Here, we implement the latter method and introduce stochastic fluctuations directly into the state variables. In natural ecosystems, environmental variability rarely acts as constant additive forces; instead, fluctuations scale with population densities. For example, larger populations experience stronger absolute disturbances, while smaller populations are less affected. To capture this ecological realism, we employ multiplicative Gaussian white noise rather than additive noise. Multiplicative noise ensures that perturbations vanish at equilibrium and increase proportionally with deviations, which is more biologically consistent for prey–predator systems. The

noise intensity parameters σ_1 and σ_2 quantify the strength of environmental disturbances on prey and predator populations, respectively. Small values of σ_i $(i = 1,2)$ represent mild seasonal fluctuations under which coexistence remains stable, whereas larger values correspond to strong disturbances (e.g., habitat loss, disease outbreaks), which may destabilize coexistence. Expanding the deterministic system (1), we derive the stochastic model as follows, based on the above assumption:

$$\begin{aligned} dx &= G_1(x,y)dt + \sigma_1(x-x^*)d\xi_t^1, \\ dy &= G_2(x,y)dt + \sigma_2(y-y^*)d\xi_t^2. \end{aligned} \tag{47}$$

Here, σ_1 and σ_2 quantify the strengths of environmental perturbations, and $\xi_t^i = \xi_i(t)(i = 1, 2)$ are independent standard Wiener processes [36]. System (47) can be written in the It $\hat{o}$ form

$$dX_t = G(t, X_t)dt + g(t, X_t)d\xi_t, X_{t0} = X_0. \tag{48}$$

The associated It $\hat{o}$ process is $X_t = (x, y)^T$ for $t > 0$. The function G represents the deterministic drift term, assumed to be continuous, whereas the diffusion matrix is given by $g = \text{diag}[\sigma_1(x-x^*), \sigma_2(y-y^*)]$, which accounts for stochastic fluctuations. Moreover, $\xi_t = (\xi_t^1, \xi_t^2)^T$ denotes a two-dimensional Wiener process whose increments $\Delta\xi_t^j = \xi_j(t+\Delta t) - \xi_j(t)$ are independent Gaussian random variables with distribution $\boldsymbol{N}(0, \Delta t)$. Since the diffusion matrix depends explicitly on the state variable X_t, System (47) is characterized by multiplicative noise.

7.1 | Stochastic Stability of the Coexistence Equilibrium

To recast System (47) about the coexistence equilibrium E^*, we introduce the perturbation variable $u(t) = (u_1(t), u_2(t))^T$, where $u_1 = x - x^*$ and $u_2 = y - y^*$. The equilibrium E^* is thereby shifted to the origin. Although mean-square asymptotic stability can be investigated for the full nonlinear stochastic model via Lyapunov function techniques, as considered in [37, 38], such an approach involves substantial analytical complexity. For tractability, we therefore confine our attention to the stochastic system obtained by linearizing (47) in a neighborhood of E^*. Accordingly, the linear approximation of (48) at the coexistence equilibrium E^* takes the following form:

$$du(t) = F_L(u(t))dt + g(u(t))d\xi(t), \tag{49}$$

where $g(u(t)) = \text{diag}[\sigma_1 u_1, \sigma_2 u_2]$ and $F_L(u(t)) = \begin{bmatrix} -\widehat{a}_{11}u_1 - \widehat{a}_{12}u_2 \\ \widehat{a}_{21}u_1 - \widehat{a}_{22}u_2 \end{bmatrix} = Mu$, $\widehat{a}_{11} = r_1 x^* - (amx^*y^*)/(b + ax^*)^2$, $\widehat{a}_{12} = x^*(m/(b + ax^*) + (Kr)/(Ky^* + 1)^2)$, $\widehat{a}_{21} = (emby^*)/(b + ax^*)^2$, $\widehat{a}_{22} = hy^*$. The coexistence equilibrium is represented by the origin $(u_1, u_2) = (0, 0)$. Let $\Omega = [(t \geq t_0) \times \mathbb{R}^2, t_0 \in \mathbb{R}^+]$, and we consider a function $\Theta(t, X) \in C^{(1,2)}(\Omega)$. That is, Θ is continuously differentiable with respect to t and twice continuously differentiable with respect to the state variable X.

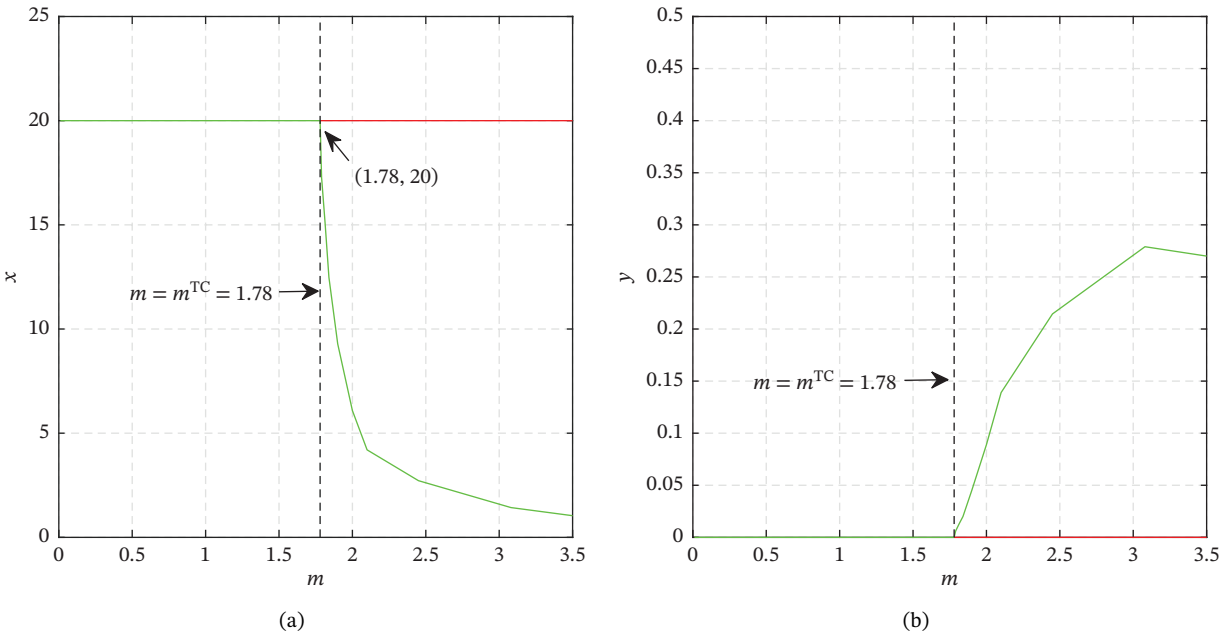

FIGURE 3 | A transcritical bifurcation occurs at $m = m_{TC} = 1.78$, where the stability of the equilibrium branches is exchanged. Numerical simulations are performed using MATLAB's ode45 solver with time step $\Delta t = 0.01$, and all other parameters are fixed at their reference parameter set (56).

TABLE 1 | Permanence results of Systems (1) and (46).

Models	Condition
(1)	$m > m^{TC} = (d(ar + br_1))/(er)$
(46)	$m > m^{TC} = (d(ar + br_1))/(er)$

TABLE 2 | The conditions for "paradox of enrichment" of the Models (1) and (46).

No.	Models	Paradox of enrichment	Conditions
1	(1)	Happens	If (21) is violated
2	(46)	Happens	If (21) is violated

$$L_\Theta(t,u) = \frac{\partial \Theta(t,u(t))}{\partial t} + f^T(u(t))\frac{\partial \Theta(t,u)}{\partial u} + \frac{1}{2}\mathrm{tr}\left[g^T(u(t))\frac{\partial^2 \Theta(t,u)}{\partial u^2} g(u(t))\right], \tag{50}$$

where

$$\frac{\partial \Theta}{\partial u} = \left(\frac{\partial \Theta}{\partial u_1}, \frac{\partial \Theta}{\partial u_2}\right)^T, \frac{\partial^2 \Theta(t,u)}{\partial u^2} = \left(\frac{\partial^2 \Theta}{\partial u_j \partial u_i}\right)_{i,j=1,2}. \tag{51}$$

In light of these circumstances, we recall the pertinent finding from [39].

Proposition 8. *If the functions $\Theta(u,t) \in C_2(\Omega)$ and L_Θ satisfy the conditions specified as follows:*

$$\widehat{r}_1|u|^\gamma \le \Theta(u,t) \le \widehat{r}_2|u|^\gamma, \tag{52}$$

$$L_\Theta(u,t) \le -\widehat{r}_3|u|^\gamma, \widehat{r}_i > 0, i = 1,2,3, \gamma > 0, \tag{53}$$

then the zero solution of equation (49) exhibits exponential γ-stability across all time intervals for $t \ge 0$.

Remark 2. When $\gamma = 2$, the criteria given in (52)–(53) guarantee that the trivial solution of (49) is exponentially stable in the mean-square sense. Furthermore, it follows from [39] that this equilibrium is also globally asymptotically stable in probability, highlighting the strengthened stability behavior associated with the choice $\gamma = 2$.

TABLE 3 | Conditions for TCB, LAS, and GAS of the Models (1) and (46).

No.	Models	Conditions	Results
1	(1)	iff $r_1 > (\mathrm{may}^*)/(ax^* + b)^2$	LAS
	(46)	iff $r_1 > (\mathrm{ma}\widehat{y}^*)/(a\widehat{x}^* + b)^2$	LAS
2	(1) & (46)	iff $m = m^{TC}$	TCB
3	(1)	iff $r_1 > (\mathrm{amy}^*)/(ax^* + b)$& $h(r_1 - (amy^*)/(ax* + b))((b + ax^*)/(be)) > (1/4)((rK)/(Ky^*+1))^2$	GAS
4	(46)	iff $r_1 > (\mathrm{am}\widehat{y}^*)/(a\widehat{x}^* + b)$	GAS

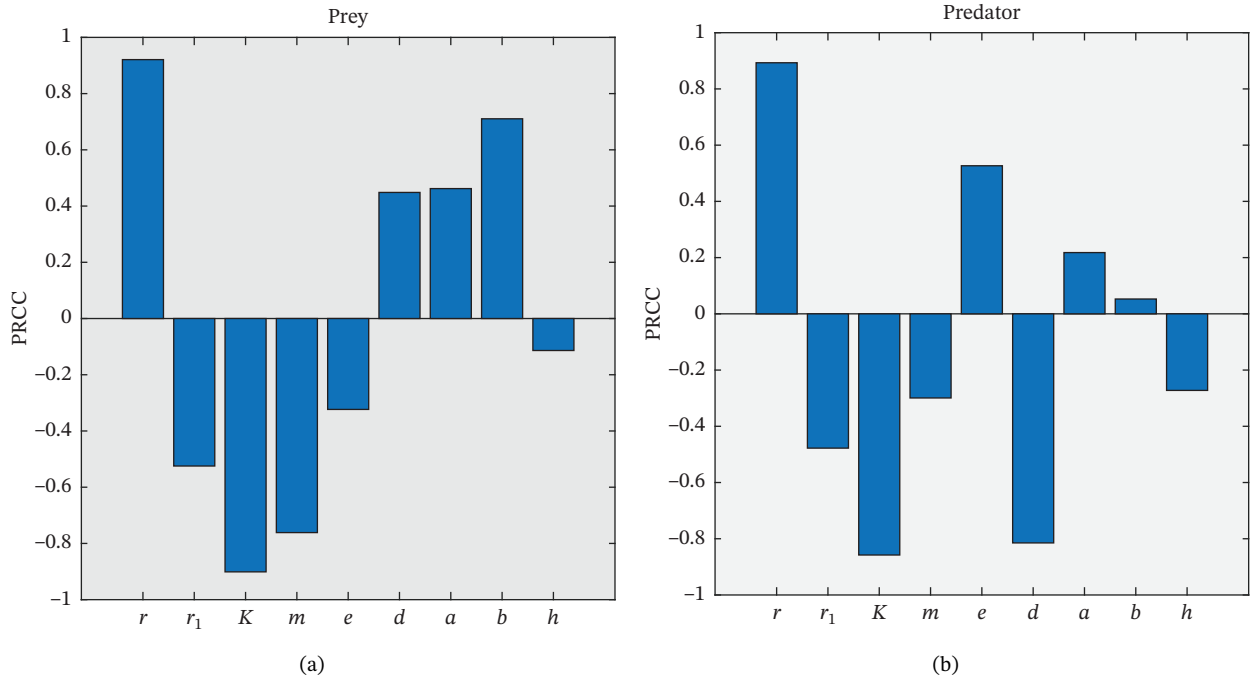

FIGURE 4 | (a-b) Analysis of parameter sensitivity for the prey (a) and predator (b); baseline parameter values are listed in equation (56).

Proposition 9. *Suppose that* $\widehat{a}_{11} < 0$. *For some* $\omega_1 > 0$, *if* $\sigma_1^2 < 2\widehat{a}_{11}$, *it follows that*

$$\sigma_2^2 < 2\widehat{a}_{22}, \tag{54}$$

where

$$\omega_1 = \frac{\widehat{a}_{12}}{\widehat{a}_{21}}, \quad \widehat{a}_{11} > 0. \tag{55}$$

Under these conditions, the zero solution of System (47) is asymptotically stable in the mean-square sense.

Proof 8. See Appendix A7. □

Remark 3. Proposition 9 provides the essential criteria for guaranteeing the stochastic stability of the coexistence equilibrium; see [40] for related results. Hence, the stability of the stochastic system is strongly influenced by the combined effects of intrinsic model parameters and the intensity of environmental variability.

8 | Numerical Simulations

This section substantiates the theoretical findings through numerical experiments that are consistent with the analytical predictions. Using simulation procedures similar to those reported in [19, 41], we examine the system dynamics and demonstrate the applicability of the derived results. For computational purposes, the parameter set is chosen as

$$\begin{aligned} &r = 4, r_1 = 0.2, K = 25, a = 1.7, b = 1.6, d = 0.03, \\ &e = 0.03, m = 3.6, h = 0.01. \end{aligned} \tag{56}$$

The coexistence equilibrium $E^* = (1.01, 0.28)$ is locally asymptotically stable and behaves as a stable focus, as illustrated in Figures 5(a).

8.1 | Effects of r

Keeping all other parameters fixed, System (1) displays oscillatory behavior around the coexistence equilibrium E^* as the intrinsic growth rate r increases from 4 to 8 (see Figures 5(b)). To illustrate the asymptotic dynamics of both species, bifurcation diagrams with respect to r are presented in Figures 6(a) and 6(b). The analysis reveals a Hopf bifurcation at $r = 6.77$ and a branch point at $r = 0.17$, indicated by (H) and (BP), respectively. The first Lyapunov coefficient at the Hopf point is −0.08, confirming that the bifurcation is supercritical and gives rise to a stable limit cycle. In contrast, a positive coefficient would correspond to an unstable periodic orbit. The branch point (BP) represents a TCB.

8.2 | Effect of r_1

When the intraspecies competition rate of prey, r_1, is low, the dynamical system becomes unstable, particularly at $r_1 = 0.16$, as shown in Figures 5(c) The influence of r_1 on system (1) is examined, and the corresponding steady-state behavior of both species is presented in Figures 7(a) and 7(b). These figures reveal that as r_1 changes, the system exhibits different behaviors. The Hopf point (H) is detected at $r_1 = 0.16$ (red star), and the associated first Lyapunov coefficient is −0.07.

8.3 | Effects of K

For lower values of the fear parameter K, the system loses stability; in particular, instability is observed at $K = 12$ (see Figures 5(d)). We demonstrate the stable-state dynamics of each population by plotting different values of K, as seen in Figures 8(a) and 8(b). Two Hopf points, indicated by red stars (H), are found at $K = 13.72$ and 0.68, respectively. The negative first Lyapunov coefficients, −0.08 and −0.008, indicate the emergence of stable periodic orbits at these points.

8.4 | Effects of m

With all parameters in System (1) fixed except m, the dynamics near the coexistence equilibrium E^* become oscillatory as m increases from 3.6 to 4; see Figure 9(a). The steady-state branches of the populations with respect to m are shown in Figures 10(a) and (b) to further clarify the equilibrium structure.

At $m = 3.99$ and $m = 1.78$, the system possesses a Hopf point (H) and a Branch point (BP), respectively. The associated Lyapunov coefficient −0.08 confirms a supercritical Hopf bifurcation, while the branch point represents a TCB (m^{TC}).

8.5 | Effects of e

Fixing all parameters in System (1) except e, the dynamics nearE^* become oscillatory as e shift from 0.03 to 0.035; see Figure 9(b). In contrast, when e decreases from 0.03 to 0.01, the system approaches the predator-free equilibrium, as depicted in Figure 9(c).

To illustrate the equilibrium response of each population, bifurcation diagrams are constructed for varying values of e (see Figures 11(a) and (b)). A Hopf bifurcation (H) occurs at $e = 0.034$, while a branch point (BP) appears at $e = 0.015$. With the first Lyapunov coefficient evaluated as −0.1, the Hopf bifurcation is supercritical and yields a stable limit cycle; in contrast, the branch point represents a TCB.

8.6 | Effect of d

The natural mortality rate of predators, denoted as d, plays a crucial role in altering the behaviors of both prey and predators. When the predator mortality rate d is low, the system exhibits unstable dynamics, particularly at $d = 0.025$ (see Figure 9(d)). Conversely, at a high mortality rate of $d = 0.08$, System (1) transitions to a predator-free equilibrium (refer to Figure 9(e)). The steady-state responses of the populations for varying d are shown in Figures 12(a) and (b). A Hopf bifurcation (H) at $d = 0.025$ (first Lyapunov coefficient −0.10) leads to a stable limit cycle, whereas the branch point (BP) at $d = 0.06$ indicates a TCB.

8.7 | Effect of b

The system exhibits oscillatory dynamics aboutE^* as the parameter b shifts from 1.6 to 1.4 (see Figure 9(f)). To examine the steady-state response of each population, bifurcation diagrams are constructed over a range of b values (Figures 12(c) and (d)). A Hopf bifurcation is detected at $b = 1.38$, where the first Lyapunov coefficient is evaluated as −0.09. These results clarify the dynamical transitions and stabilization patterns of the populations as b varies, with all other parameters held fixed.

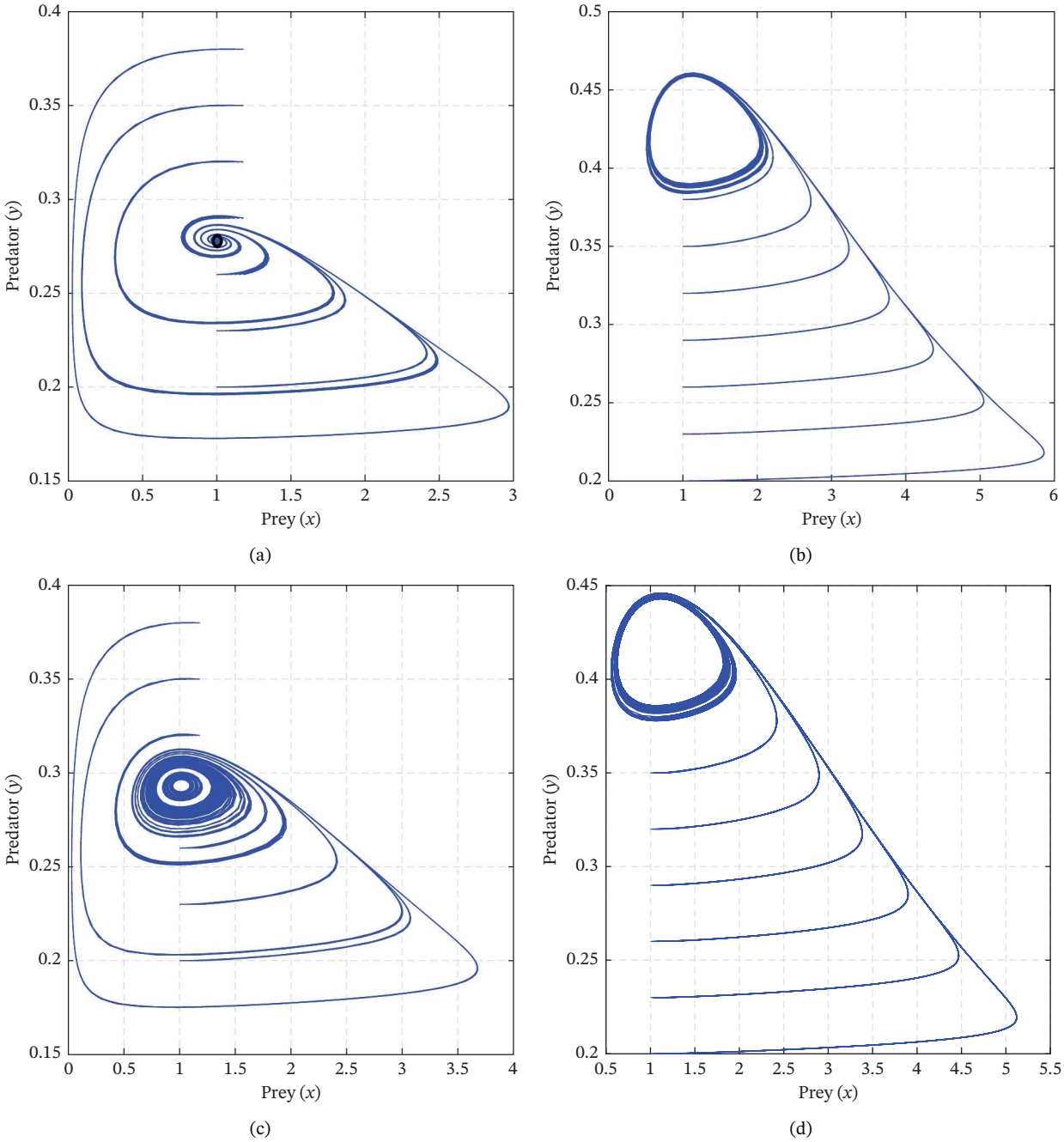

FIGURE 5 | (a) The global stability of the coexistence equilibrium around E^* for the reference parameters given in (30). (b–d) The system exhibits stable limit cycles for $r = 8$, $r_1 = 0.16$, and $K = 12$, respectively.

8.8 | Bistability and the Hopf-Bifurcation Region

The bifurcation diagrams in Figures 13(a), 13(b), 13(c) and 13(d) and Figures 14(a), 14(b), 14(c), provide a detailed representation of the dynamic behavior of System (1) in relation to the parameters m, K, r, r_1, e, b, and d. Figures 2(a), 2(b), 2(c), 2(d) illustrate two-parameter bifurcation diagrams for the combinations $m - K$, $m - r_1$, $m - b$, and $r_1 - K$. In System (1), a BTB arises when the critical parameter configuration causes both eigenvalues to vanish simultaneously. Such a bifurcation reflects a qualitative transition in the system dynamics, potentially giving rise to new attractors or equilibrium configurations. The generalized Hopf (GH) bifurcation, characterized by the vanishing of the first Lyapunov coefficient, constitutes an important local bifurcation in a two-parameter family of autonomous ordinary differential equations. At this point, the equilibrium becomes critical, and a pair of purely imaginary eigenvalues emerges, indicating a fundamental alteration in the phase portrait, often resulting in the formation of limit cycles or other complex dynamical behaviors.

Finally, different dynamic regimes are depicted with varying colors in the bifurcation diagrams for parameter combinations $m - K$, $m - r$, $m - e$, $r - K$, $K - e$, and $m - h$, as shown in Figures 15(a), 15(b), 15(c), 15(d), 15(e), and 15(f). Table 4 presents a concise overview of the results, detailing the

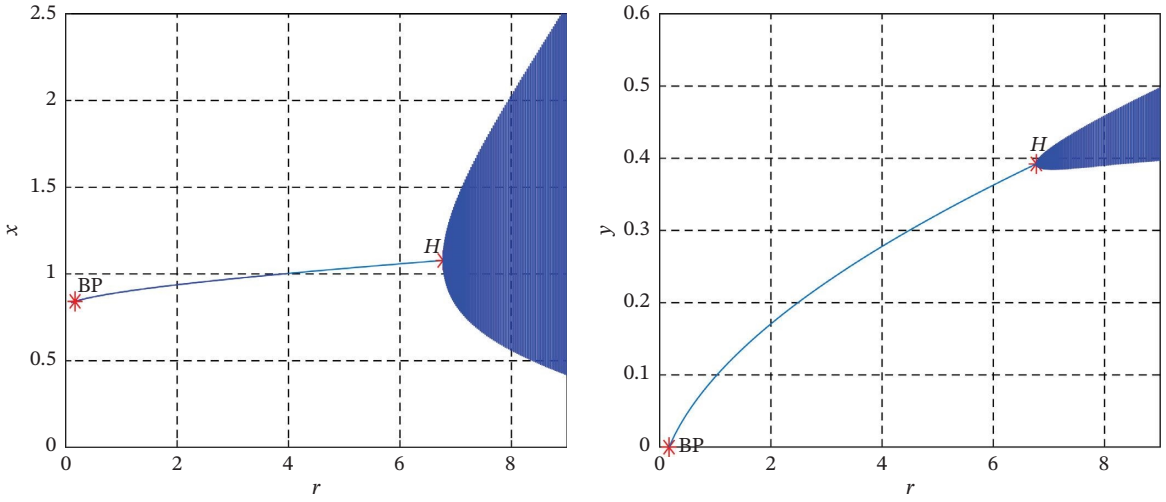

FIGURE 6 | (a-b) The trajectory illustrates the prey and predator dynamics under variations in r, revealing stable limit cycles emerging from the Hopf (H) bifurcation.

qualitative properties of the equilibrium states in the proposed predator–prey model.

8.9 | Environmental Fluctuations

Next, we examine the system's dynamic behavior when subjected to environmental disturbances. We utilize the Euler–Maruyama (EM) method, implemented through MATLAB software, to perform numerical simulations of the stochastic differential equation (22). By applying an appropriate Lyapunov function (36), we determined the conditions necessary for the asymptotic stability of E^* in a mean-square sense for Equation (22). These conditions are influenced by σ_1, σ_2, and the model system parameters. With $\sigma_1 = 0.0003$ and $\sigma_2 = 0.0003$ representing the intensities of environmental disturbances and parameters aligned with those used in a deterministic system, each species coexists and remains stochastically stable (see Figures 16(a) and 16(b)). Subsequently, when the environmental fluctuation values are increased to $\sigma_1 = 0.002$ and $\sigma_2 = 0.002$, the coexistence equilibrium becomes unstable (see Figures 16(c) and 16(d)). Figure 17(a) and 17(b) show the stationary distributions of prey $x(t)$ and predator $y(t)$ for the stochastic system (47), with varying values of $\sigma_i (i = 1, 2)$. The probability-density functions of $x(t)$ and $y(t)$ are depicted by red smoothed curves. Figures 17(a) and 17(b) reveal noticeable differences in the stationary distributions with different magnitudes of $\sigma_i (i = 1, 2)$, remarkably resembling a normal distribution when $\sigma_i = 0.0003 (i = 1, 2)$.

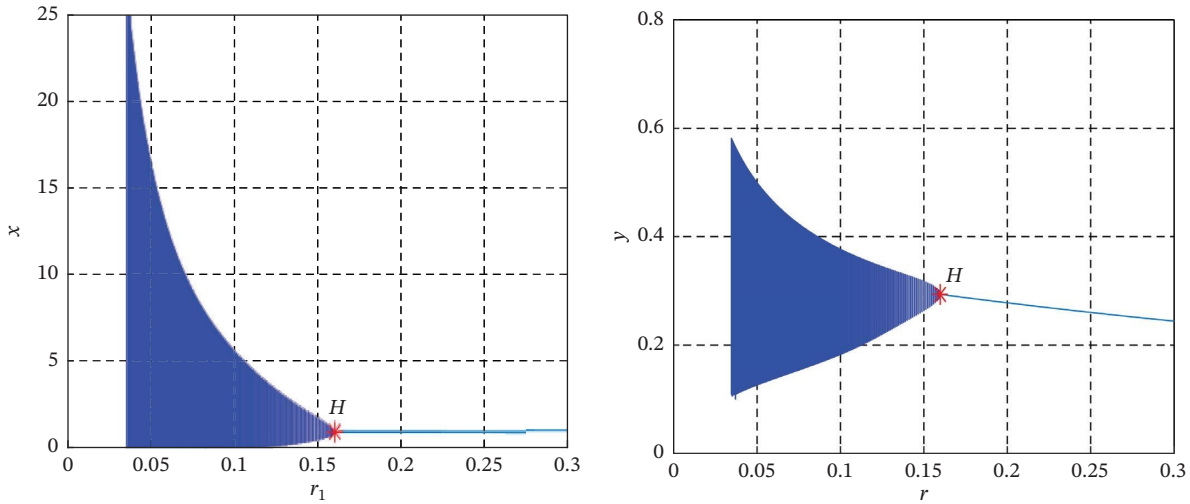

FIGURE 7 | (a-b) The trajectory illustrates the prey and predator dynamics under variations in r_1, revealing stable limit cycles emerging from the Hopf (H) bifurcation.

9 | Rich Dynamics of System (1): Numerical Lyapunov Exponents Perspective

While continuous-time predator–prey models are suitable for analytical studies, many ecological processes—such as seasonal reproduction, generational turnover, population censuses, and harvesting—occur at discrete time intervals. Discretizing the continuous model therefore provides a more realistic framework for describing population dynamics across successive generations or seasons. From a dynamical perspective, discrete-time systems can exhibit complex behaviors, including multistability, period-doubling bifurcations, and chaos, even when the corresponding continuous system remains stable. These dynamics are ecologically meaningful, as they may represent irregular population fluctuations, outbreaks, or sudden collapses observed in nature. Mathematically, the discrete system is obtained via an appropriate time discretization of the continuous model, preserving positivity and biological feasibility of solutions. This formulation enables a detailed numerical investigation of bifurcation structures and Lyapunov exponents, thereby complementing the continuous analysis and offering deeper insight into the long-term ecological consequences of fear-induced nonlinearities.

Here, we analyze the behavior of the Lyapunov exponent thorough numerical exploration withintwo-dimensional parameter space. The outcomes unveil the presence of countless self-repeating shrimp-shaped and Arnold-tongue patterns that correspond to periodic attractors.

Calculating Lyapunov characteristic exponents is essential for understanding system dynamics. These exponents quantify the rate at which nearby trajectories either diverge or converge. The presence of periodic attractors can be determined by analyzing the stability of limit sets and the sensitivity to initial conditions. Furthermore, the Lyapunov exponents' perspective offers a foundational approach to studying and understanding dynamical systems' intrinsic unpredictability and complexity. By quantifying the divergence of trajectories, they provide crucial insights into the nature and degree of chaos, enhancing our ability to analyze and interpret the behavior of complex systems across various scientific domains.

Therefore, to judge the long-term behavior of the model, we use the Lyapunov exponent, which serves as an indicator to analyze different prey–predator interactions. Here, we have drawn two bi-parameter Lyapunov exponents to identify the transactions between various parameters. In these transactions, we have focused on only three behaviors: periodic, quasiperiodic, and chaotic dynamics. These dynamics are classified in terms of the three values of the Lyapunov exponent.

The zero value of the Lyapunov exponent represented by the green color indicates the quasiperiodic dynamics; the positive values of Lyapunov exponents are defined by the blue shades, signifying the chaotic behavior; and the pink shades in the plot mark the periodic regions corresponding to the negative value of the Lyapunov exponent. In the quasiperiodic region, the populations oscillate in a nonrepeating but bounded fashion. The population neither stabilizes into an equilibrium point nor shows divergence into chaos.

At the same time, chaos represents unpredictable behavior, and a slight change causes the collapse of the population. Meanwhile, periodicities are regions of the population where the population exhibits stable or oscillatory behavior.

We want to check System (1) for complex dynamics at the discretized space of points. We must first discretize Model (1). We aim to present the chaotic and periodic behavior of the model at the discretized grid of points. These plots indicate richer dynamics of Model (1) and provide a roadmap for the discrete form, mathematically showing the existence of chaos and other interesting results.

Using Euler's method, System (1) can be written as

$$\left.\begin{aligned} x_{n+1} &= x_n + h_1\left[\frac{rx_n}{Ky_n+1} - r_1x_n^2 - \frac{mx_ny_n}{ax_n+b}\right] \\ y_{n+1} &= y_n + h_1\left[\frac{emx_ny_n}{ax_n+b} - dy_n - hy_n^2\right] \end{aligned}\right\}, \tag{57}$$

where h_1 is the step size. We choose different parameters to analyze the predator–prey model's dynamic behavior in a two-dimensional parameter plane. When the system parameters were varied, periodic and chaotic diagrams were obtained. Here, we use a numerical iterative approach to solve the difference equations with different initial conditions to compute the Lyapunov exponent of the system for different pairs of parameters. Figure 18 shows the dynamic behavior of the model as the parameters r and m are varied with the following set of values: $\{h = 2.8, h_1 = 0.5, K = 1.9, r_1 = 1.6, a = 2.6, b = 1.2, e = 0.9, d = 0.1(r, m) \in [9.7, 10.3] \times [17.5, 19.1]\}$, with initial conditions $(x_0, y_0) = (0.8, 0.9)$. The color bar indicates different values of the Lyapunov exponent. From the color bar, the positive Lyapunov exponent represents chaos. The negative Lyapunov exponent represents the periodic solutions. In Figure 18, we observe interesting periodic structures of well-known Arnold tongues. The structure of the tongues is similar in that the roots of the tongues are in the chaotic region, while the tips of the tongues are in the quasiperiodic regions. To illustrate hidden Arnold tongues above the larger tongues, we present the zoomed-in view of Figure 18 in Figure 20. Here, we observe two different patterns of periodicity in the form of Arnold tongues. In Figure 20(a), Arnold tongues are in an irregular pattern, while in Figure 20(b), Arnold tongues are in a sequence with a pointed side in the downward direction.

Similarly, to observe the complex dynamics between the parameters a and K, we have drawn the Lyapunov exponent between these two parameters in Figure 19. For Figure 20, we choose $(0.8, 0.9)$ as an initial condition. The remaining parameters are fixed as $m = 2.3, h = 0.2, h_1 = 0.9, r_1 = 0.6, b = 1.9, e = 0.9, d = 2.5, r = 1.9, a \in [1.9, 2.7], K \in [1, 18]$. We follow the same color code for Figure 19 to represent the chaotic dynamic between parameters a and b. In this plot, we observe two types of periodic patterns: Arnold tongues and shrimps. The Arnold tongues can be seen from the top right side of the plot, while the shrimps can be seen from the bottom left side of the plot. To better view these two existing periodic structures, we present the zoomed-in view of Figure 19 in Figure 21. Figure 21(a) represents the series of Arnold tongues in the deep sea of the chaos, while Figure 21(b) represents the shrimps in the deep chaotic region. Figure 22 represents a clear view of a large shrimp with a collection of small shrimps near it.

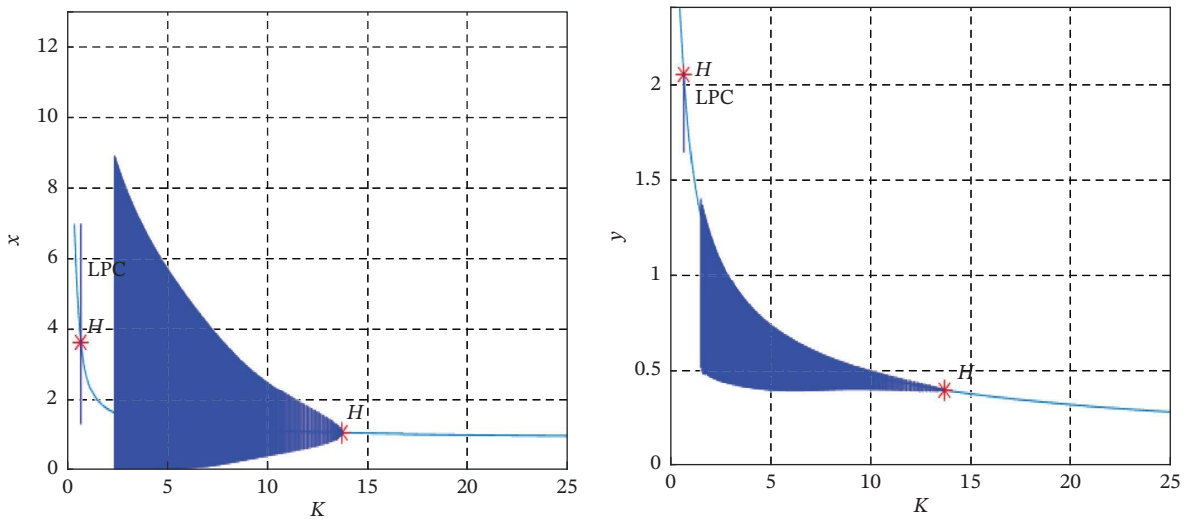

(a) (b)

FIGURE 8 | (a-b) Trajectories of prey and predator as K varies, highlighting stable limit cycles from the Hopf (H) points.

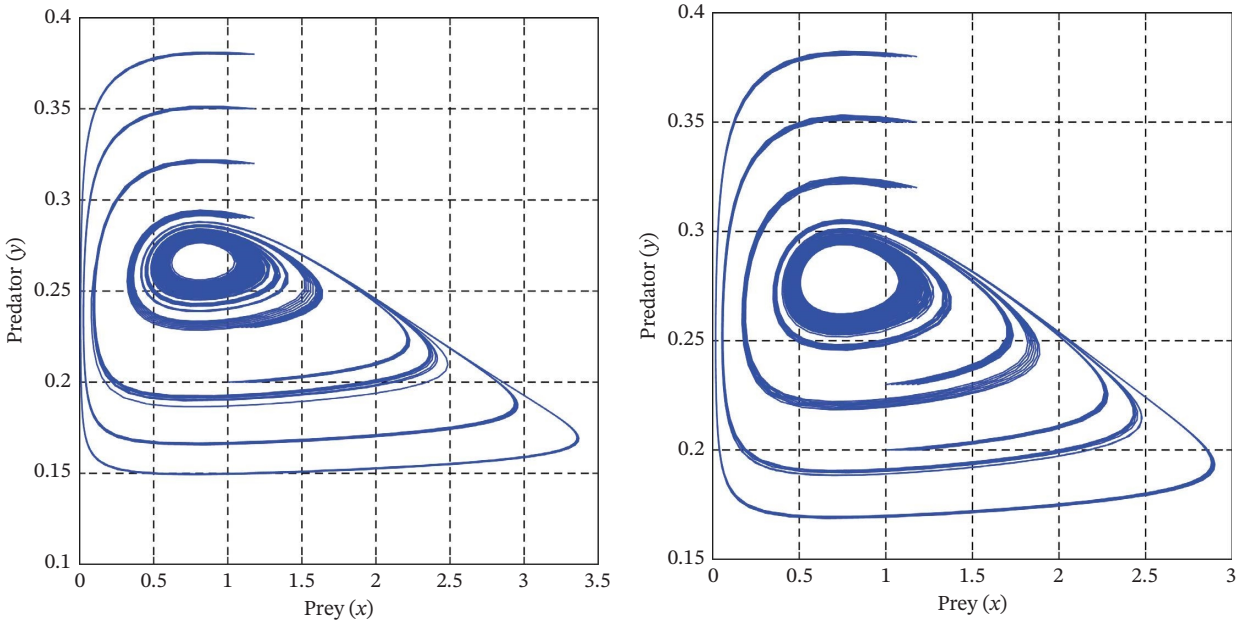

(a) (b)

FIGURE 9 | (Continued)

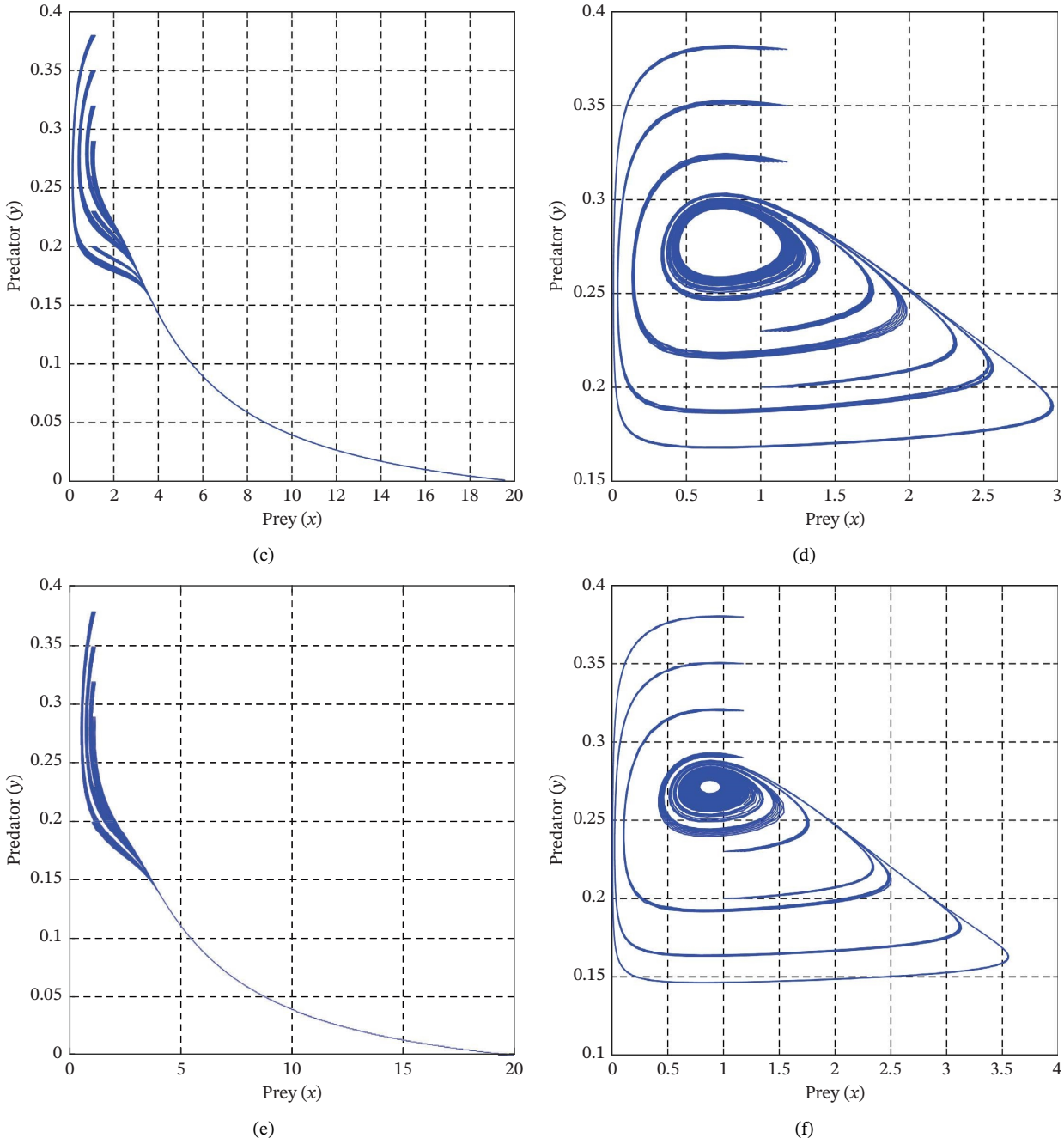

FIGURE 9 | (a-b) The system exhibits stable limit cycles for $m = 4$, $e = 0.035$ respectively. (c) System exhibits predator free equilibrium for $e = 0.01$. (d) For $d = 0.025$, the picture displays oscillatory behavior around E^*. (e) The figure displays predator-free stable equilibrium around E_1 for $d = 0.08$. (f) System exhibits stable limit cycles for $b = 1.4$.

Thus, we have usedMATLAB to compute the Lyapunov spectrum of a smooth dynamical system. Through the two-parameter Lyapunov exponents, we have observed the complex dynamics in the discretized model. The complex nature of the model represents its dynamical richness. The analysis and understanding of these dynamical shifts help protect populations from upcoming environmental risks and hazards.

Example 1. In this example, we will confirm the occurrence of Hopf bifurcation in System (1). If we choose the following parameter values, the forward Hopf bifurcation occurs when r is chosen as a bifurcation parameter:

$$K = 1.8, r_1 = 0.35, m = 3.19, a = 2.9, b = 1.81, \\ e = 0.9, d = 0.1, h = 0.01, r \in [0.1, 0.5], \tag{58}$$

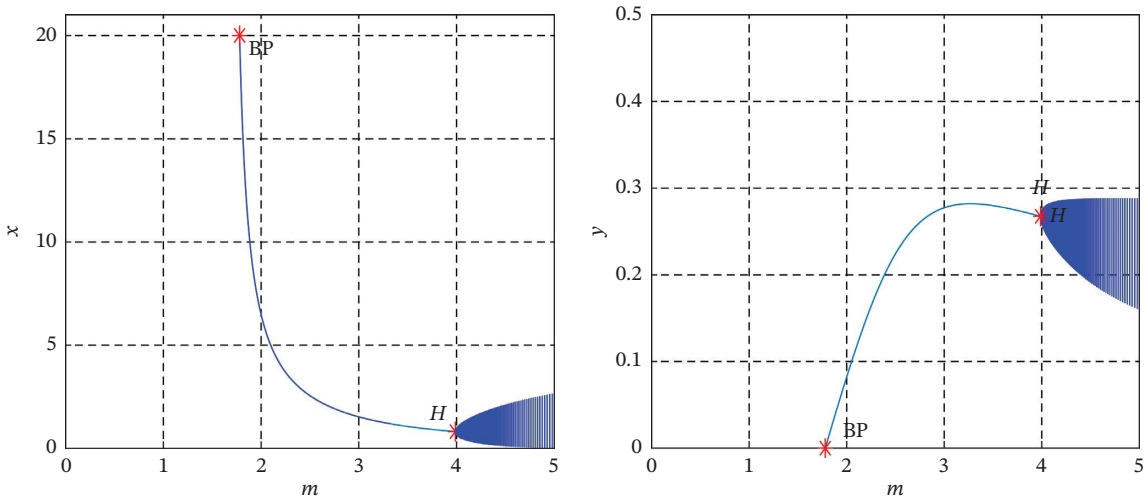

FIGURE 10 | (a-b) The trajectory illustrates the prey and predator dynamics under variations in m, revealing stable limit cycles emerging from the Hopf (H) bifurcation.

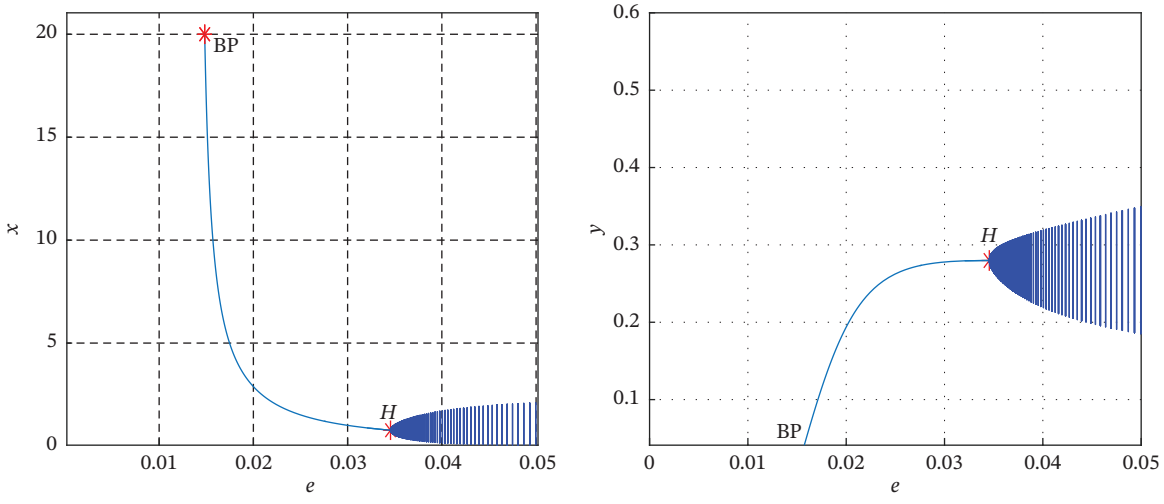

FIGURE 11 | (a-b) The trajectory illustrates the prey and predator dynamics under variations in e, revealing stable limit cycles emerging from the Hopf (H) bifurcation.

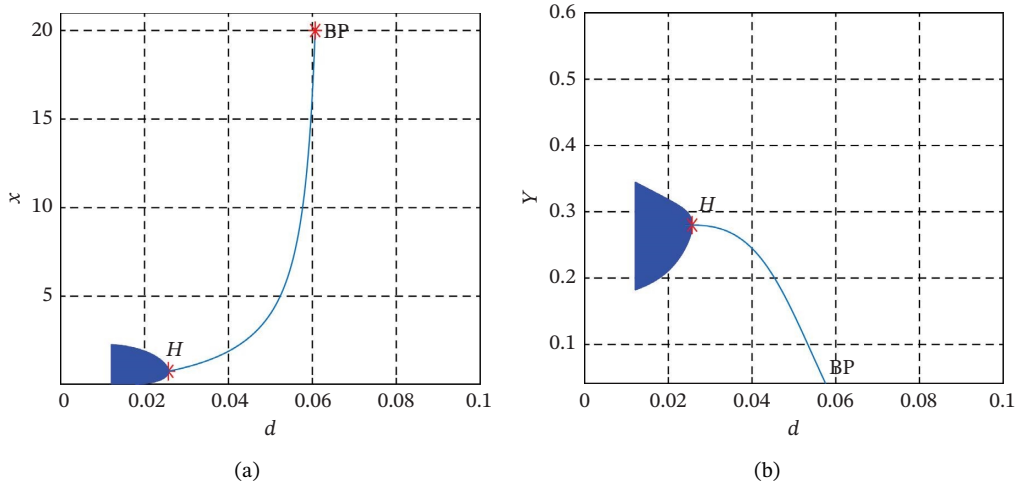

FIGURE 12 | (Continued)

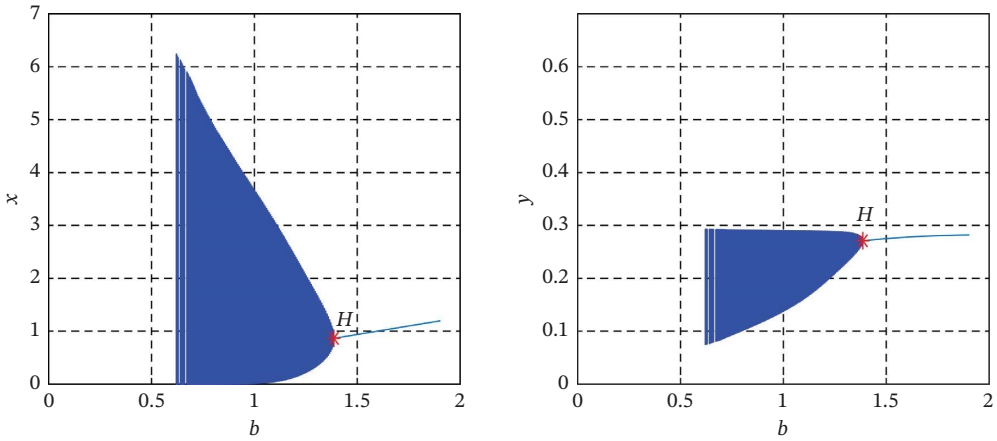

FIGURE 12 | (a–d) Trajectories of prey and predator under variations in d and b, respectively, showing stable limit cycles arising from the Hopf (H) bifurcation.

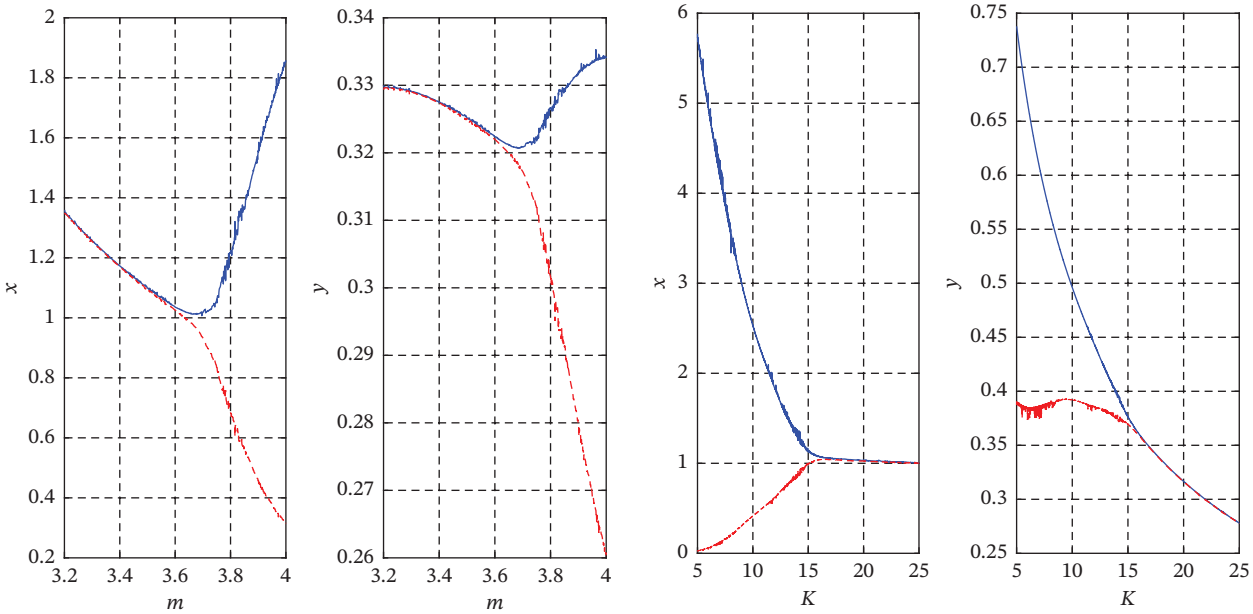

FIGURE 13 | (Continued)

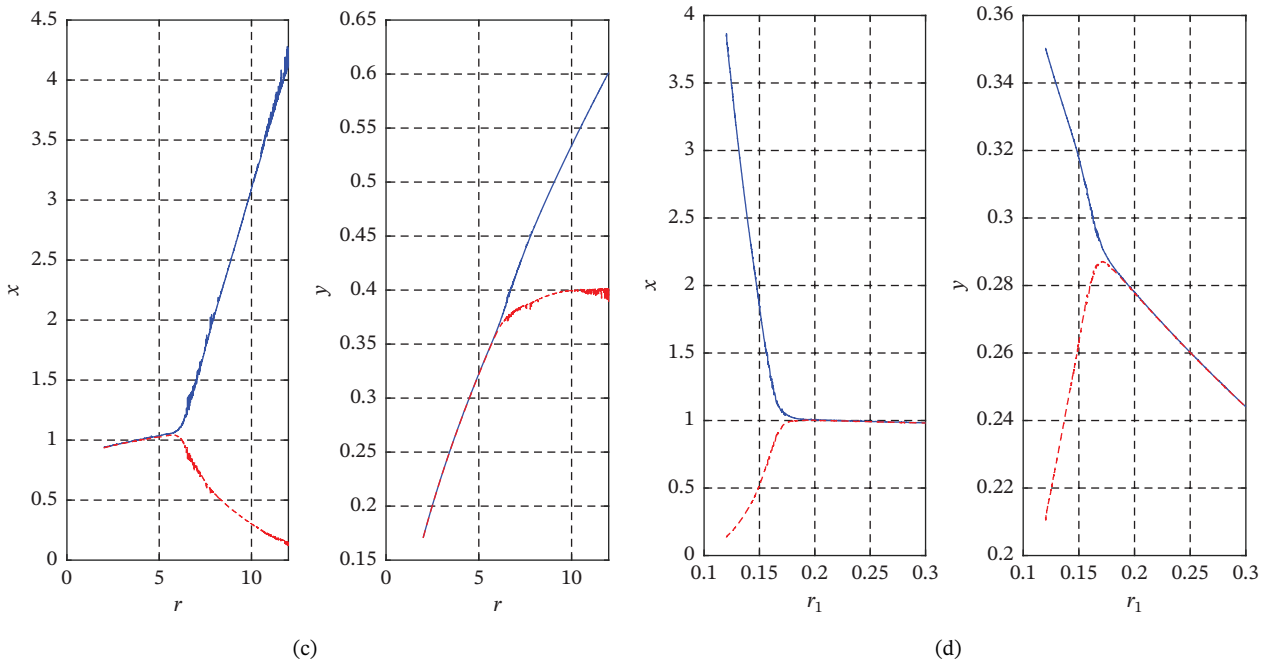

FIGURE 13 | (a–d) Bifurcation diagram in terms of m, K, r, and r_1 respectively: prey (left), predators (right).

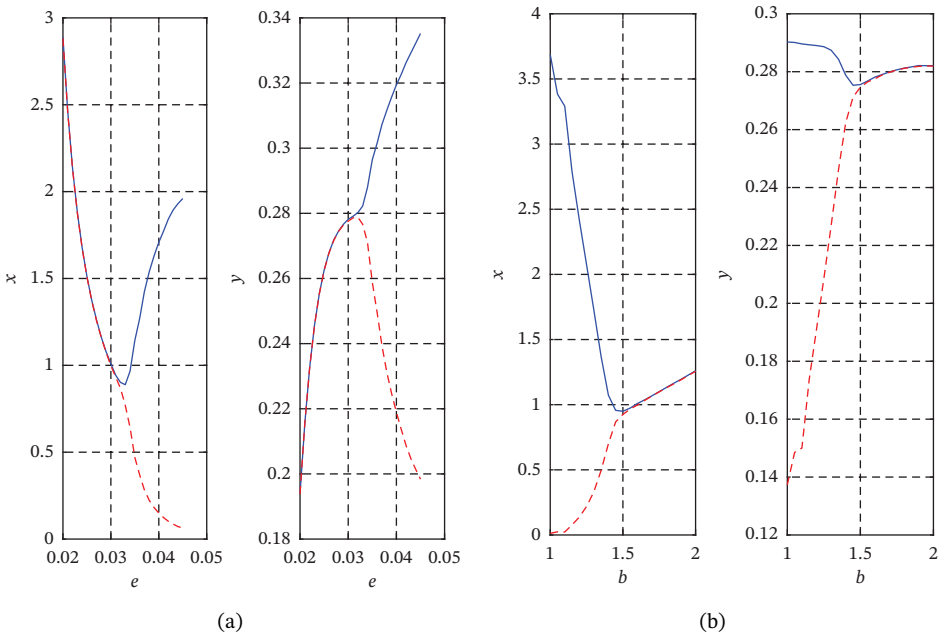

FIGURE 14 | (Continued)

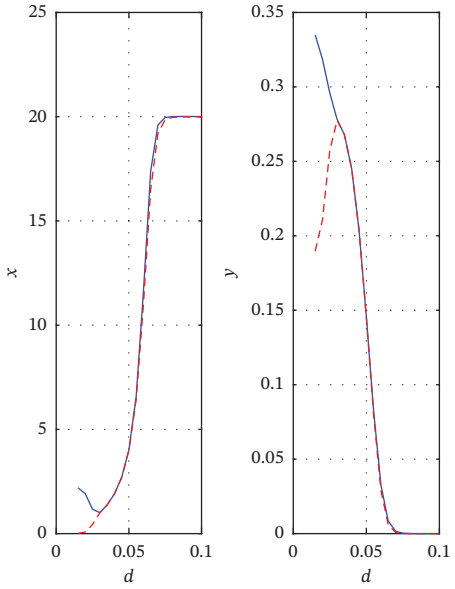

(c)

FIGURE 14 | (a–c) Bifurcation diagram in terms of e, b, and d, respectively: prey (left), predators (right).

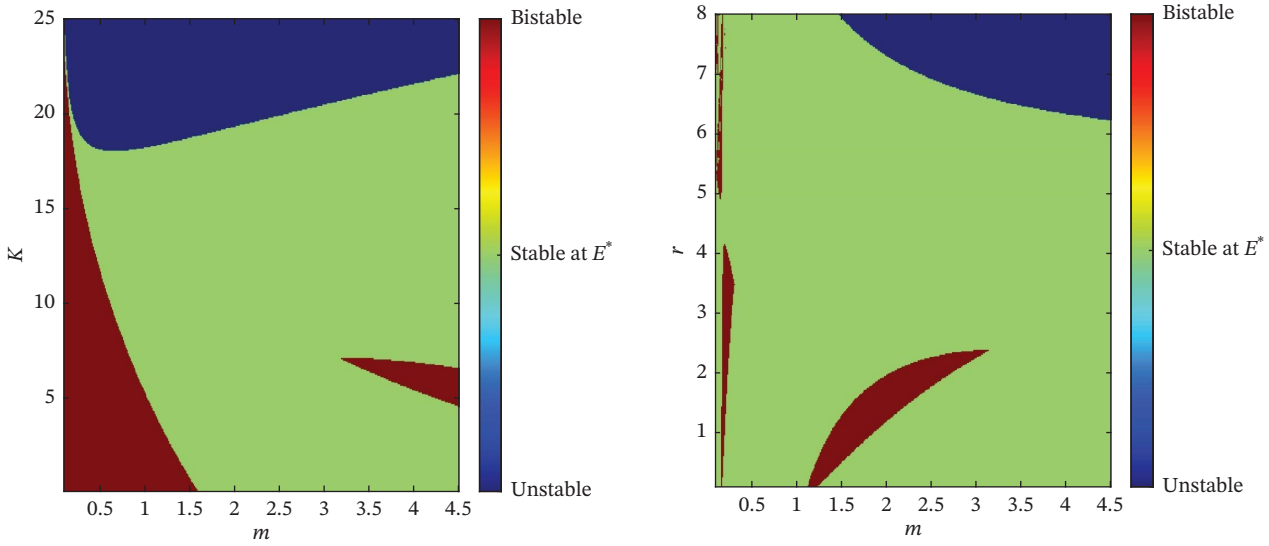

(a) (b)

FIGURE 15 | (Continued)

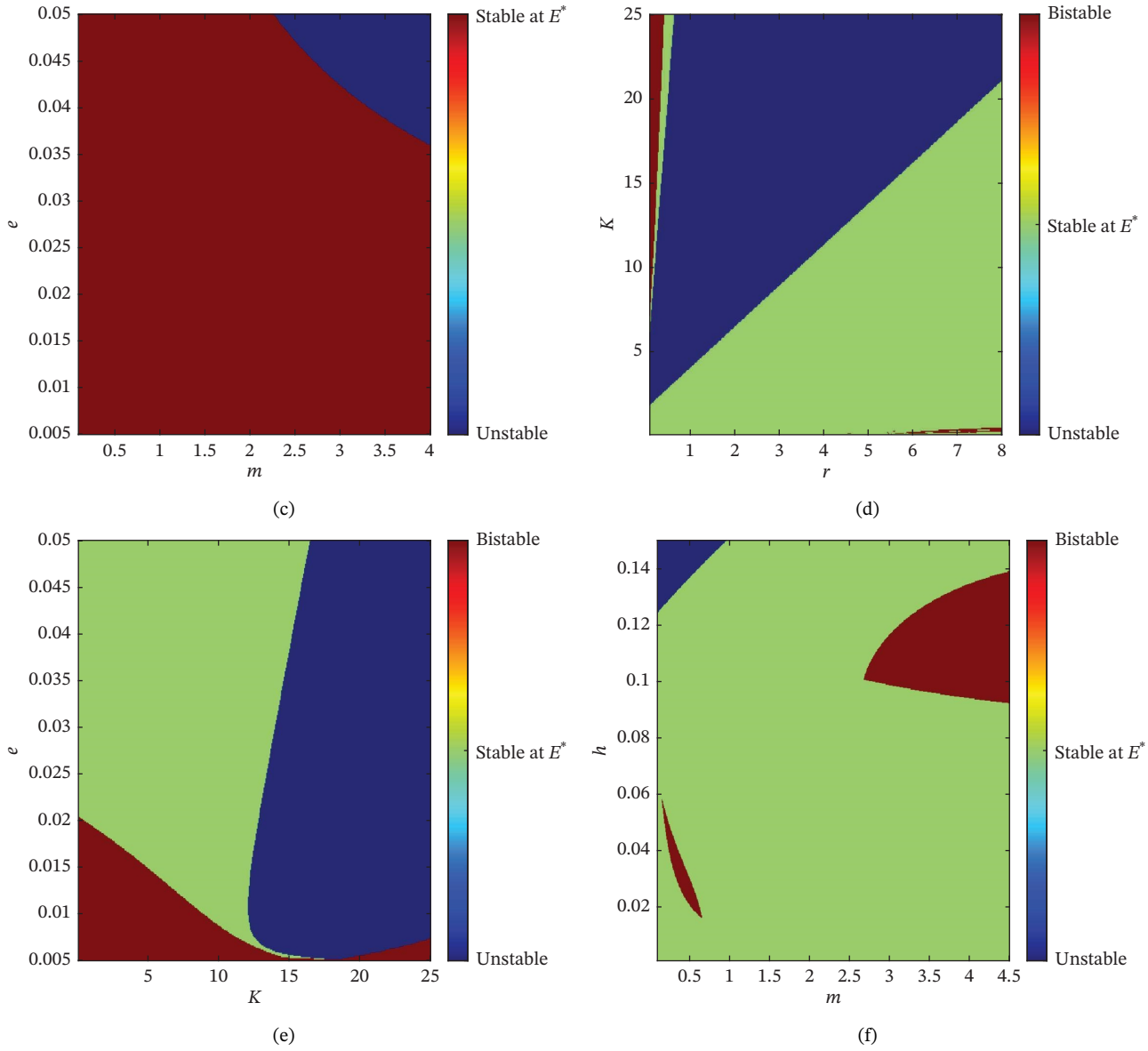

FIGURE 15 | (a–f) Dynamical regimes of System (1) depicted in the two-parameter planes (m, K), (m, r), (m, e), (r, K), (K, e), and (m, h).

with $(x_0, y_0) = (0.1, 0.1)$. *Particularly, the system becomes unstable near* $r \approx 0.31907032$. *For parameter values,*

$$K = 1.8, r_1 = 0.35, m = 3.19, a = 2.9, b = 1.81, e = 0.9, \\ d = 0.1, h = 0.01, r = 0.31907032, \tag{59}$$

the Jacobian matrix at the equilibrium point $(0.0712426377677212, 0.1426779168610621)$ *is given as follows:*

$$\begin{pmatrix} 0.00142667 & -0.1386 \\ 0.182317 & -0.00142678 \end{pmatrix}. \tag{60}$$

The characteristic function of (32) is

$$C(\mu) = \mu^2 + 0.025267037665026477. \tag{61}$$

Since we are using an approximate value of r (i.e., $r \approx 0.31907032$) therefore, the coefficient of $\mu \approx 0$. One can also find a better approximation or exact value of r to get the coefficient of μ exactly equal to zero. The eigenvalues are $\{\pm 0.158956i\}$ with the real part approximately zero. Hence, the mathematical existence of the Hopf bifurcation is satisfied. The phase plots given in Figure 23 confirm that the direction of the bifurcation is forward, while the corresponding time-series plots in Figure 24 also ratify the findings.

10 | Discussion

In recent years, increasing attention has been directed toward the influence of fear on predator–prey dynamics, establishing fear ecology as an important area of research. This area of research is now gaining paramount importance as it delves into the intricate dynamics of ecosystems and their complex behaviors. This paper delved into the complicated dynamics of a predator–prey model with a Holling type II functional response, where the fear of predation risk significantly affects the birth rate of the prey. Moreover, the model comprehensively accounts for intraspecific

TABLE 4 | Characteristic of equilibrium points.

Parameters	Values	Eigenvalues	Equilibrium points
r	6.77	$(\pm 0.124i)$	Hopf (H)
	0.17	$(0, -0.169)$	Branch point (BP)
r_1	0.159	$(\pm 0.108i)$	Hopf (H)
K	13.72	$(\pm 0.122i)$	Hopf (H)
	0.68	$(\pm 0.139i)$	Hopf (H)
m	3.99	$(\pm 0.12i)$	Hopf (H)
	1.78	$(o, -4)$	Branch point (BP)
e	0.03	$(\pm 0.12i)$	Hopf (H)
	0.014	$(0, -4)$	Branch point (BP)
d	0.025	$(\pm 0.11i)$	Hopf (H)
	0.025	$(0, -4)$	Branch point (BP)
b	1.38	$(\pm 0.11i)$	Hopf (H)
$m - K$	(3.75, 0.476)	$(\pm 0.14i)$	Generalized Hopf (GH)
$m - r_1$	(2.36, 0.009)	$(\pm 0.03i)$	Generalized Hopf (GH)
$r_1 - K$	(0.16, 0.68)	$(\pm 0.13i)$	Generalized Hopf (GH)
$m - b$	(1.94, 0.08)	$(\pm 0.03i)$	Generalized Hopf (GH)
	(1.86, 0.0)	(0,0)	Bogdanov–Takens (BT)

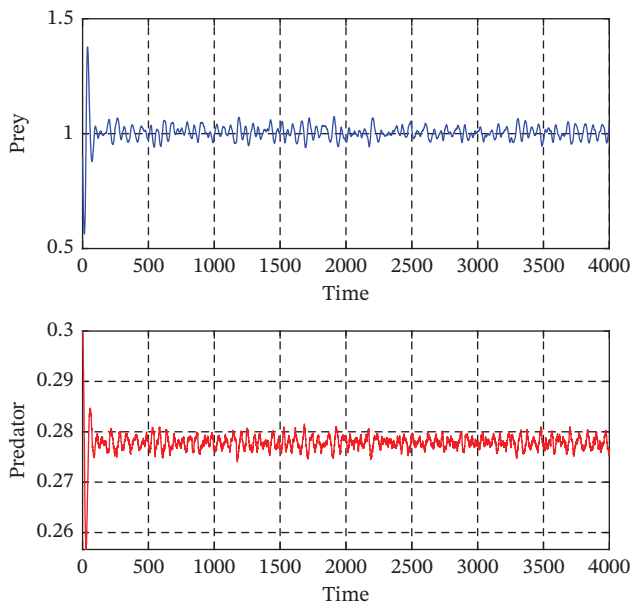

(a)

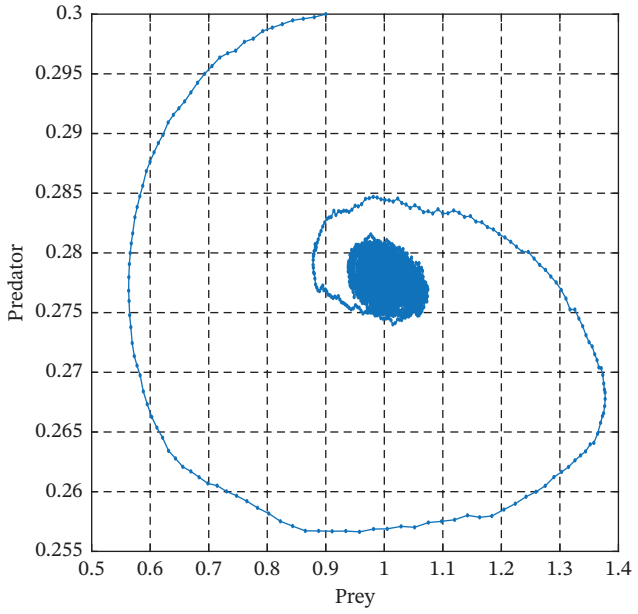

(b)

FIGURE 16 | (Continued)

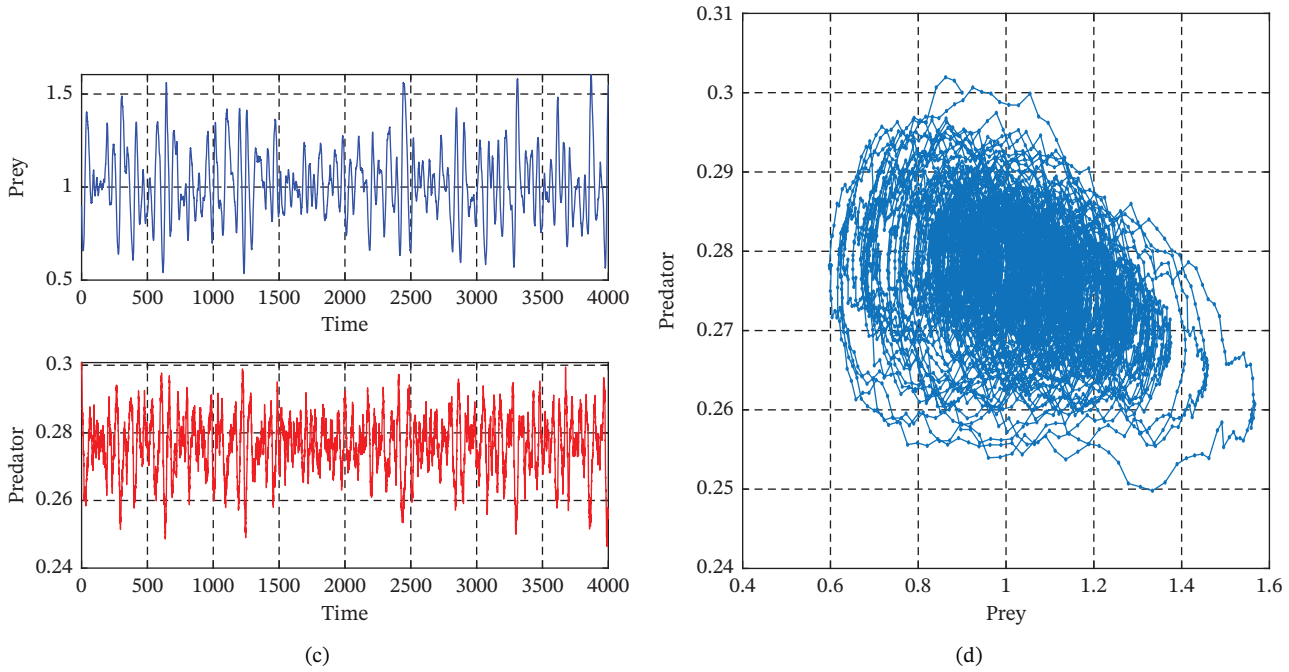

FIGURE 16 | (a-b) The graphical results confirm the stochastic stability of the system for noise intensities $\sigma_1 = 0.0003$ and $\sigma_2 = 0.0003$. (c-d) The numerical illustrations indicate that the system exhibits stochastic instability when $\sigma_1 = 0.002$ and $\sigma_2 = 0.002$.

competition within the predator population, a natural phenomenon driven by the limitations of available resources in the ecosystem. An analysis of these interacting components provides deeper understanding of the intricate dynamics of ecological systems and clarifies the significant influence of fear on predator–prey interactions.

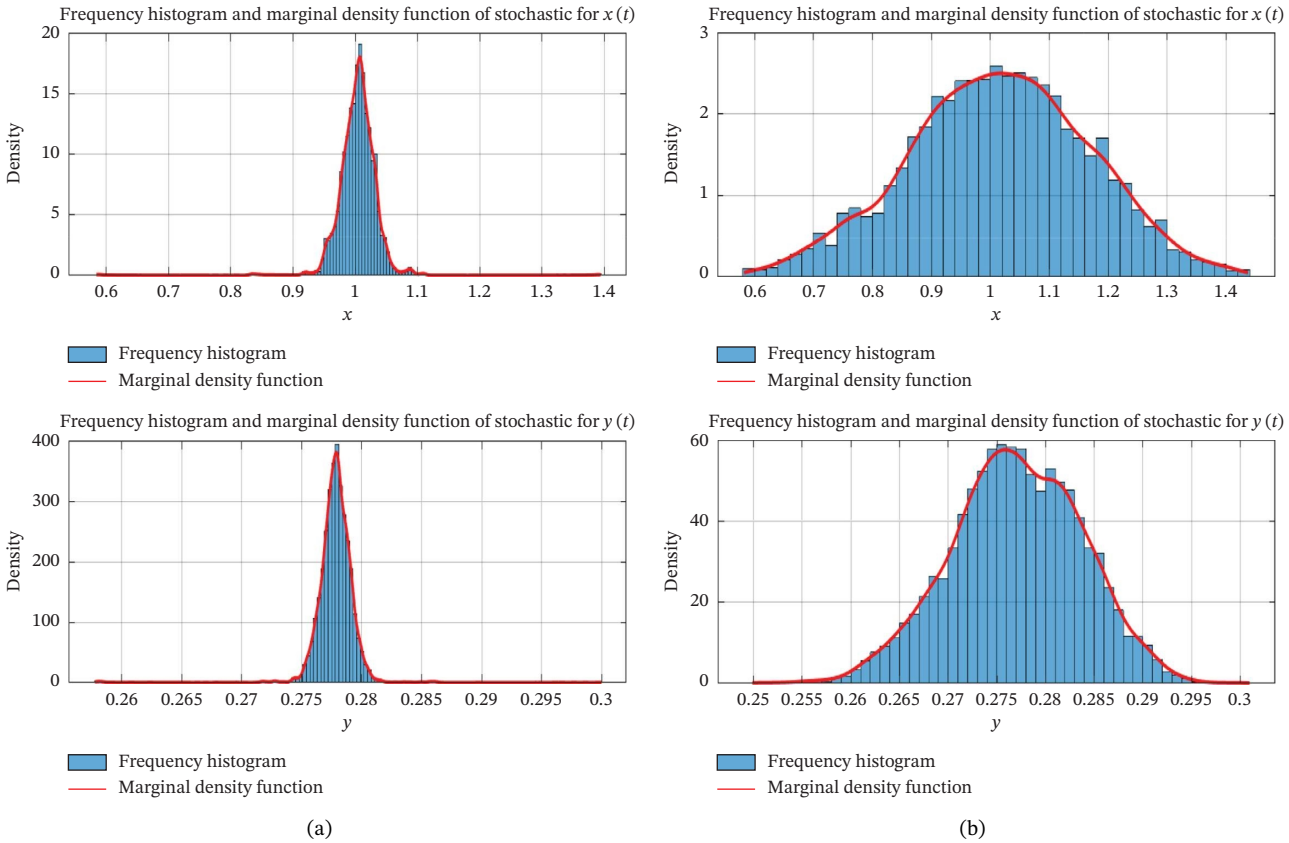

FIGURE 17 | Histogram of the probability density function for $x(t)$ and $y(t)$ for the stochastic system (22) with two different values of σ_i $(i = 1,2)$; (a) $(\sigma_1 = 0.0003, \sigma_2 = 0.0003)$; (b) $(\sigma_1 = 0.002, \sigma_2 = 0.002)$; the probability density functions of $x(t)$ and $y(t)$ are represented by the red smoothed curves.

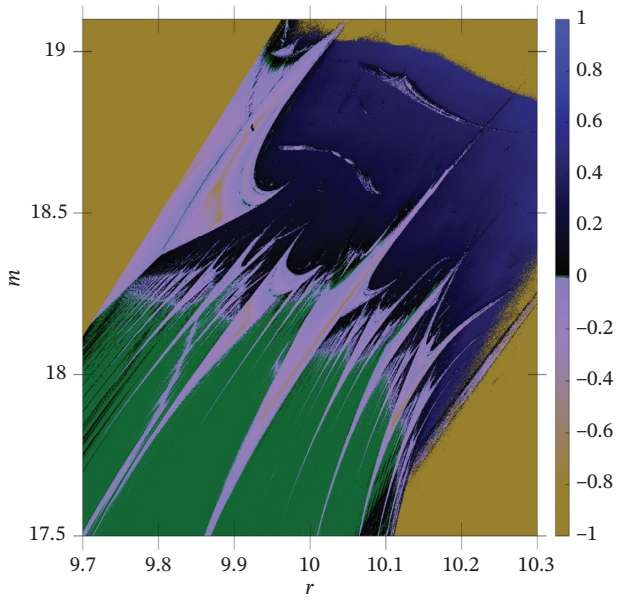

FIGURE 18 | Lyapunov exponent for $h = 2.8, h_1 = 0.5, K = 1.9, r_1 = 1.6, a = 2.6, b = 1.2, e = 0.9, d = 0.1, (r, m) \in [9.7, 10.3] \times [17.5, 19.1]$ with initial conditions $(x_0, y_0) = (0.8, 0.9)$.

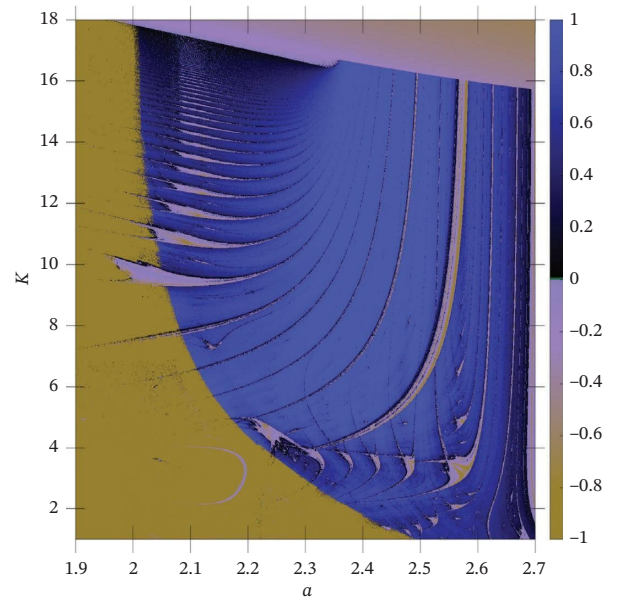

FIGURE 19 | Lyapunov exponent for $m = 2.3, h = 0.2, h_1 = 0.9, r_1 = 0.6, \quad b = 1.9, e = 0.9, d = 2.5, r = 1.9, a \in [1.9, 2.7], K \in [1, 18], x_0 = 0.8, y_0 = 0.9$.

Our research yields noteworthy coexistence outcomes within the system. The proposed system is biologically well-posed, since all solutions initiated in the positive quadrant remain non-negative and uniformly bounded for all future time. The instability of the trivial equilibrium excludes total extinction, independent of parameter selection. The local dynamics around the feasible equilibria are rigorously analyzed, and sufficient criteria for both local and global stability of the interior equilibrium are established, thereby clarifying the system's persistence and robustness. In addition, the model undergoes significant qualitative transitions, including TCB and Hopf bifurcation, which enrich the dynamical behavior and reveal complex evolutionary patterns. These findings contribute significantly to our understanding of the model's behavior and its potential implications for ecological systems.

The detected bifurcations are ecologically meaningful. In particular, the TCB alters the predator-extinction equilibrium E_1, converting it from an unstable state to a stable configuration. Additionally, we identify six specific parameters responsible for inducing the Hopf bifurcation. Through rigorous analysis, we have thoroughly examined the stability of the resulting limit cycle and verified our findings by employing numerical simulations and computing the first Lyapunov number. These findings enhance the understanding of the system's dynamics and provide meaningful implications for ecological processes.

One of the key novelties of the current study lies in incorporating intraspecific competition among prey and predator populations, reducing their growth rate. The predator's consumption rate, the predator's efficiency rate to consume prey into a new predator, and the intrinsic growth rate of prey play pivotal roles in regulating oscillations within the system and facilitating the emergence of a stable coexistence equilibrium point. Consequently, our findings suggest an opposite influence of both the fear factor and consumption rate within the predator population on the system's stability, mainly when the predation process adheres to the Holling type II response function. The system's stability is also influenced similarly by factors such as intraspecies competition for prey and the natural mortality rate of predators.

Furthermore, conducting a comparative analysis between the systems represented by Equations (1) and (46), the permanence outcomes of these systems are summarized in Table 1. On the other hand, Table 2 proves that when Condition (21) is violated, Systems (1) and (46) still have the "paradox of enrichment." Table 3 also shows that the qualitative behaviors of Systems (1) and (46) attain TCB, LAS, and GAS around their axial and coexistence equilibrium point. Note that "level of fear" has no influence on the trivial (E_0) and boundary equilibrium (E_1) of System (1). However, the fear effect is crucial to the system's local and global stability at E^*. Further, our observation indicates that there is a possibility of two coexistence equilibria in System (1), while only one coexistence equilibrium can exist in System (46). In other words, modification of System (46) by introducing an extra term, "level of fear," enables richer dynamics.

Based on our mathematical analysis, we determine that when fear levels of predator or intraspecies competition of prey are high, they can stabilize the predator–prey system by preventing the existence of periodic solutions. Conversely, when fear levels or intraspecies competition of prey are relatively low, they can trigger the emergence of limit cycles through Hopf bifurcation. However, low degrees of fear can prompt multiple limit cycles through subcritical Hopf bifurcations, prompting a bistability peculiarity. This result is contrasted with exemplary predator–prey models, which overlook the cost of fear where Hopf bifurcations are normally supercritical. Hopf bifurcations in our model can be supercritical and subcritical by choosing various parameters. We used numerical simulations to investigate the connections between fear and other biologically related parameters, including birth rate, death rate, and interspecies

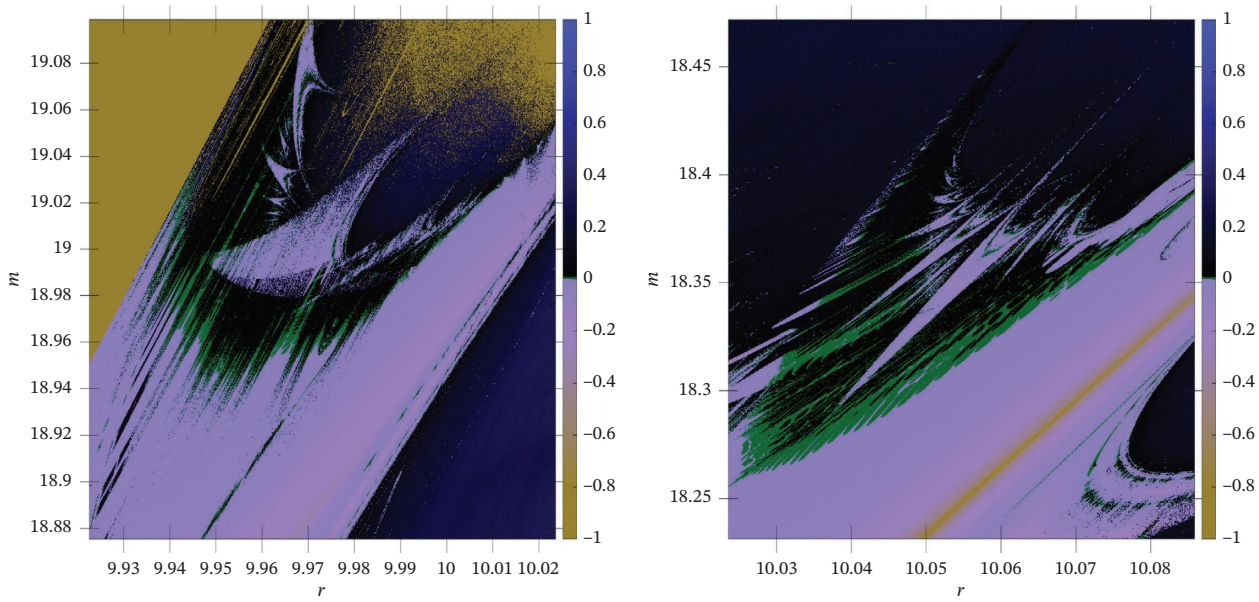

FIGURE 20 | Local amplification of the plot in Figure 18.

competition, which further exhibits the effect of fear on predator–prey interactions. For instance, we discover that when a Hopf bifurcation occurs, a rise in fear can cause the direction of the bifurcation to change from supercritical to subcritical when the birth rate of prey rises correspondingly. Numerical results further indicate that increasing the prey growth rate or the predator death rate reduces the prey population's sensitivity to predation risk. Still, prey will develop more robust predator defenses as predator attack rates rise. In addition, a higher intrinsic growth rate of prey, predator consumption rate, and efficiency in converting consumed prey into new predators can result in limit cycles through Hopf bifurcation. The two-parameter bifurcation analysis further reveals the presence of both generalized Hopf and BTBs in the system. The validity of these findings is confirmed through appropriate numerical simulations. Consequently, our findings suggest an opposite influence of both the

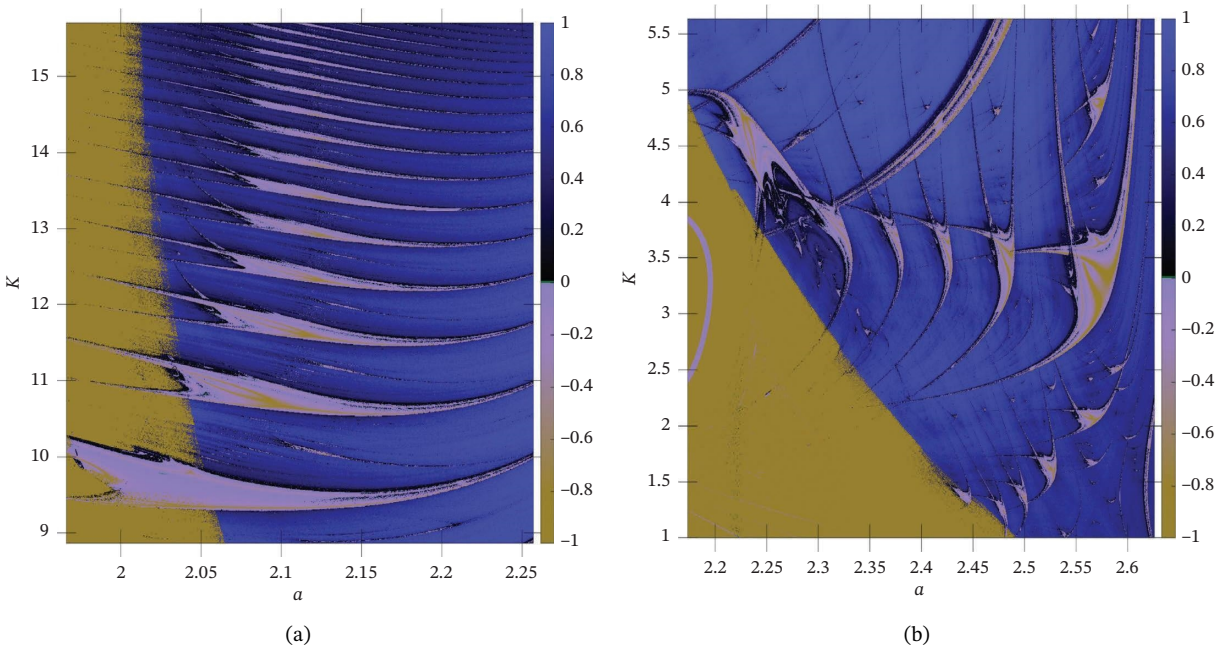

FIGURE 21 | Local amplification of the plot in Figure 19 representing the Arnold tongues and shrimps.

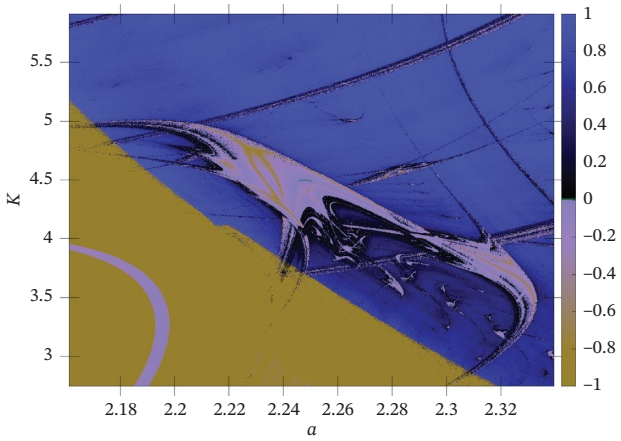

FIGURE 22 | The zoomed view of Figure 19 represents a clear view of shrimp with the collection of small shrimps aside from it.

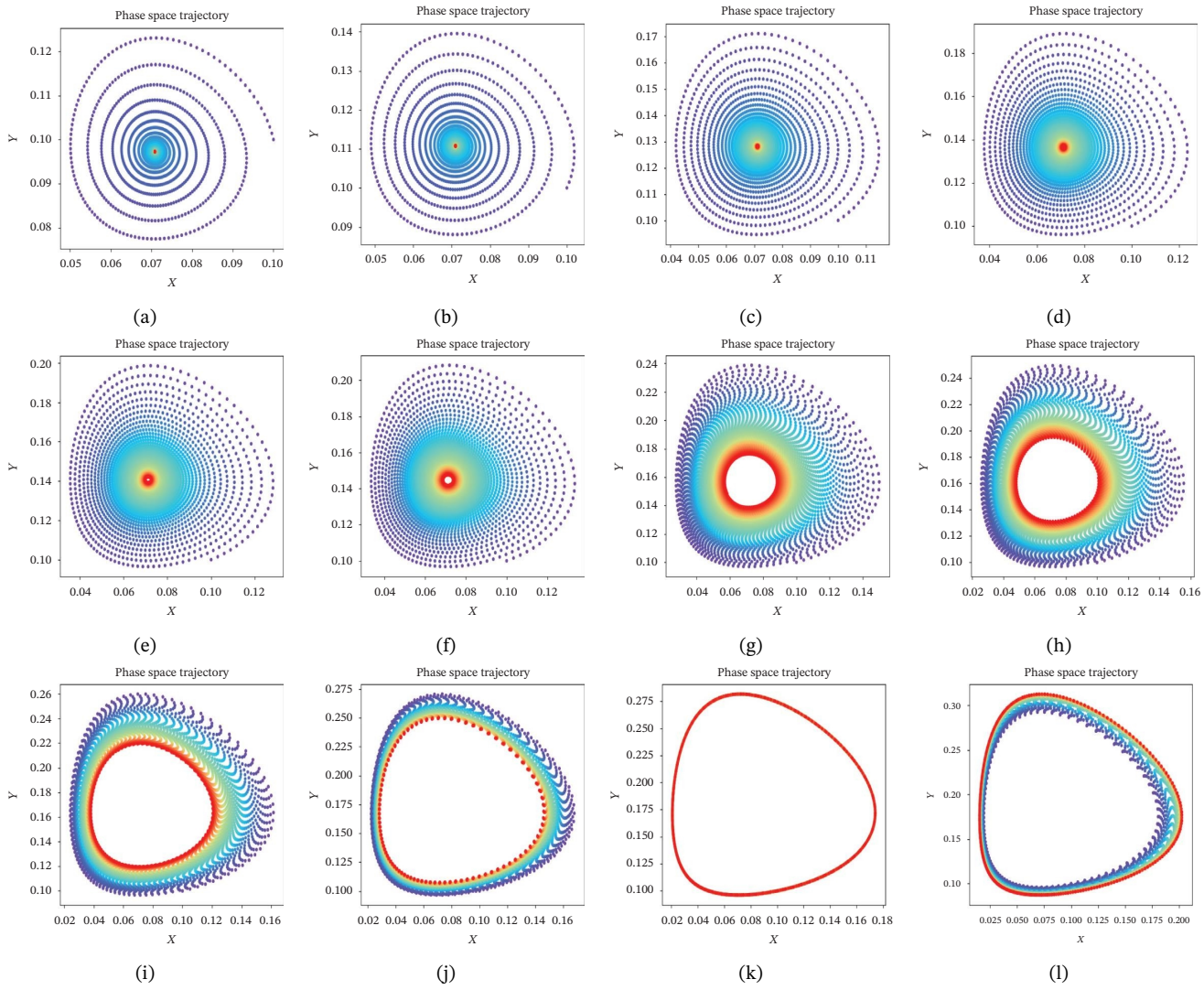

FIGURE 23 | (Continued)

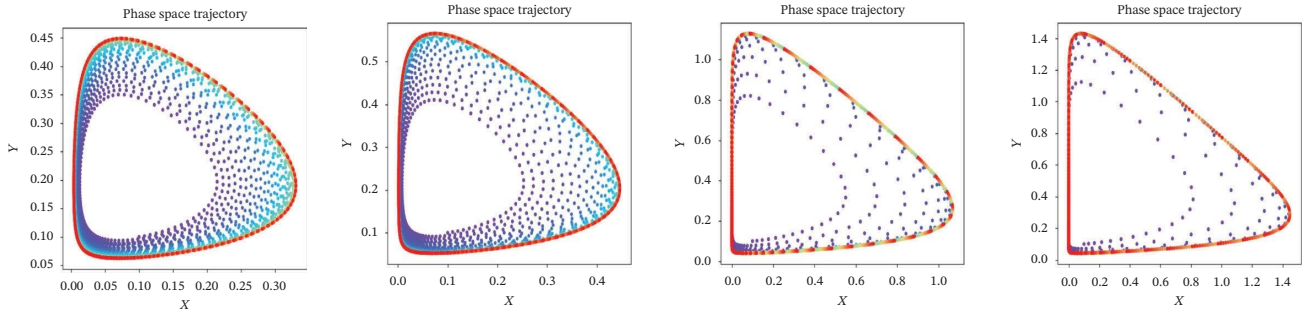

(m) (n) (o) (p)

FIGURE 23 | Phase plots for different values of r. (a) $r = 0.21$. (b) $r = 0.24$. (c) $r = 0.28$. (d) $r = 0.3$. (e) $r = 0.31$. (f) $r = 0.32$. (g) $r = 0.35$. (h) $r = 0.36$. (i) $r = 0.37$. (j) $r = 0.38$. (k) $r = 0.39$. (l) $r = 0.4$. (m) $r = 0.45$. (n) $r = 0.5$. (o) $r = 0.8$. (p) $r = 1.0$.

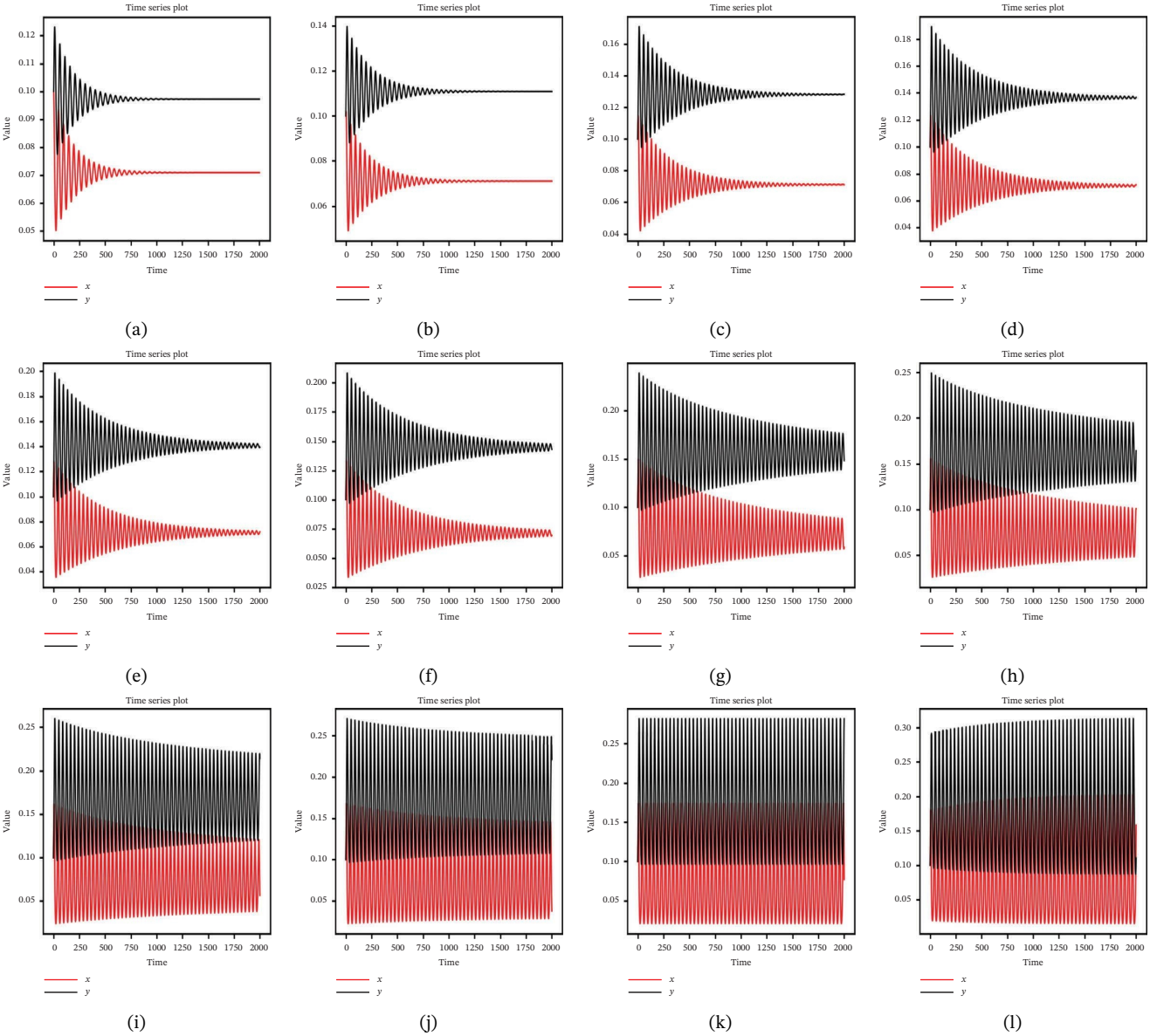

(a) (b) (c) (d)

(e) (f) (g) (h)

(i) (j) (k) (l)

FIGURE 24 | (Continued)

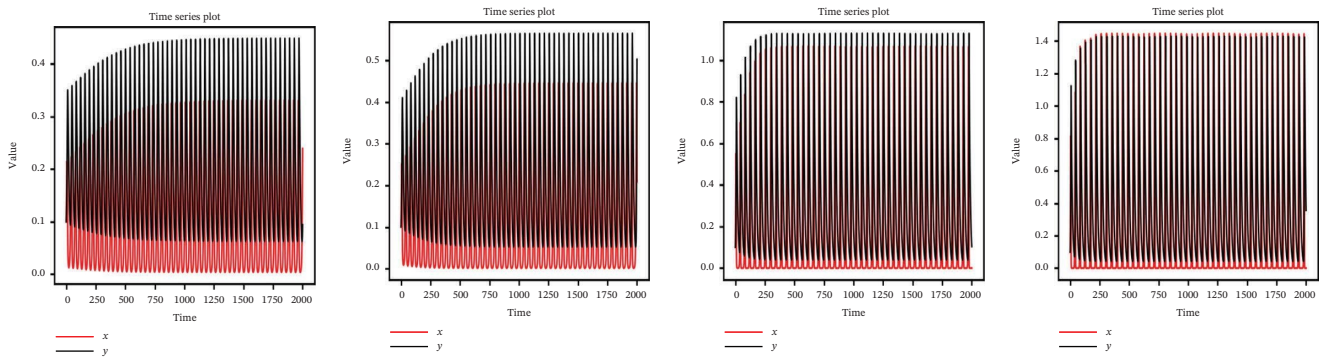

FIGURE 24 | Time-series plots for different values of r. (a) $r = 0.21$. (b) $r = 0.24$. (c) $r = 0.28$. (d) $r = 0.3$. (e) $r = 0.31$. (f) $r = 0.32$. (g) $r = 0.35$. (h) $r = 0.36$. (i) $r = 0.37$. (j) $r = 0.38$. (k) $r = 0.39$. (l) $r = 0.4$. (m) $r = 0.45$. (n) $r = 0.5$. (o) $r = 0.8$. (p) $r = 1.0$.

fear factor and consumption rate within the predator population on the system's stability, particularly when the predation process adheres to the Holling type II response function.

Environmental noise is a critical factor influencing ecological systems, particularly through its impact on predator–prey dynamics. It introduces randomness and unpredictability, which can significantly alter the behavior and stability of these systems. This noise stems from unpredictable changes in environmental factors such as resource availability and habitat quality. These factors directly affect the growth rates of both predator and prey populations, leading to fluctuating population sizes [42].

In ecological modeling, environmental noise is often contrasted with deterministic models, which assume a predictable set of conditions and outcomes. While deterministic models provide a simplified view of ecological interactions, they fail to capture the inherent variability and uncertainty present in natural systems. Stochastic simulations, on the other hand, incorporate randomness and are thus more adept at representing the complexity of ecological dynamics [43]. One of the significant impacts of environmental noise is its influence on population stability. Low-intensity noise can promote stochastic asymptotic stability, where populations tend to fluctuate around a stable state over time. This stability is crucial for maintaining ecological balance, as it ensures that neither predators nor prey are driven to extinction due to random environmental variations [44]. Conversely, high-intensity noise can lead to significant oscillations and increased unpredictability in population dynamics. Such conditions may drive populations away from equilibrium, potentially leading to extinction events or drastic shifts in community structure. For example, suppose a prey population experiences a sudden drop due to a resource shortage. In that case, predator populations may also decline due to a lack of food, demonstrating how interconnected and sensitive these dynamics can be [45]. To ensure the sustainability of ecological systems amidst environmental noise, it is essential to maintain specific constraints on random variations and model parameters. These constraints help mitigate the potentially destabilizing effects of high-intensity noise and support the resilience of ecological systems. By carefully managing environmental variability, conservation efforts can enhance the stability and sustainability of ecosystems [20]. Moreover, understanding the role of environmental noise in ecological systems is vital for predicting future changes under climate-change scenarios. As climate change is expected to increase the frequency and intensity of environmental variability, anticipating its effects on ecological dynamics becomes increasingly essential. Incorporating stochastic elements into ecological models can provide valuable insights into how these systems might respond to future environmental challenges [46]. In conclusion, environmental noise is a fundamental component of ecological systems, affecting predator–prey dynamics and population stability. Low-intensity environmental noise may enhance the stability of the system, whereas higher noise levels can generate substantial oscillations and increase dynamical unpredictability. Understanding and managing environmental noise through stochastic modeling is crucial for ensuring the resilience and sustainability of ecosystems in the face of ongoing environmental changes.

In addition, the study includes numerical findings on a dissipative standard map. When considering dissipation, the phase space structure is altered, with the elliptic fixed points being replaced by attracting fixed points. Analyzing the Lyapunov exponent shows that the parameter space (a, K) is highly diverse and contains numerous self-similar shrimp-shaped and Arnold structures. These structures correspond to periodic attractors and are found within a large region associated with chaotic attractors.

Lyapunov exponents are critical tools in the field of dynamical systems and chaos theory, providing insights into the behavior of complex systems. They measure the rate at which nearby trajectories in a dynamical system diverge or converge, thus indicating the presence and extent of chaos. A positive Lyapunov exponent typically suggests chaos, where small differences in initial conditions can lead to vastly different outcomes, a hallmark of chaotic systems. The current article also emphasizes the importance of calculating Lyapunov characteristic exponents to understand discrete-time predator–prey system dynamics. These exponents measure the rate at which nearby trajectories diverge or converge and can determine the presence of chaotic attractors. In a detailed numerical investigation within a two-dimensional parameter space, the behavior of the Lyapunov exponent reveals numerous self-repeating shrimp-shaped and Arnold patterns corresponding to periodic attractors. These configurations arise within a broader parameter domain characterized by chaotic behavior.

Moreover, concerning predator–prey interactions, factors such as spatial effects, delays, and environmental noise play a crucial role due to the foraging behaviors of both prey and predators. Although these potential extensions are biologically significant and intriguing, their complexities are challenging, leaving them as fascinating subjects for future study.

Funding

Stacey R. Smith? was supported by an NSERC Discovery Grant.

Conflicts of Interest

The authors declare no conflicts of interest.

Data Availability Statement

The data that support the findings of this study were generated through numerical simulations of the proposed mathematical model. All parameter values used for the simulations are provided within the article.

References

1. T. K. Kar, "Stability Analysis of a Prey–Predator Model Incorporating a Prey Refuge," *Communications in Nonlinear Science and Numerical Simulation* 10, no. 6 (2005): 681–691, https://doi.org/10.1016/j.cnsns.2003.08.006.

2. S. Creel and D. Christianson, "Relationships Between Direct Predation and Risk Effects," *Trends in Ecology and Evolution* 23, no. 4 (2008): 194–201, https://doi.org/10.1016/j.tree.2007.12.004.

3. S. L. Lima, "Predators and the Breeding Bird: Behavioral and Reproductive Flexibility Under the Risk of Predation," *Biological Reviews* 84, no. 3 (2009): 485–513, https://doi.org/10.1111/j.1469-185x.2009.00085.x.

4. M. Haque, S. Sarwardi, S. Preston, and E. Venturino, "Effect of Delay in a Lotka–Volterra Type Predator–Prey Model With a Transmissible Disease in the Predator Species," *Mathematical Biosciences* 234, no. 1 (2011): 47–57, https://doi.org/10.1016/j.mbs.2011.06.009.

5. M. Haque, N. Ali, and S. Chakravarty, "Study of a Tri-Trophic Prey-Dependent Food Chain Model of Interacting Populations," *Mathematical Biosciences* 246, no. 1 (2013): 55–71, https://doi.org/10.1016/j.mbs.2013.07.021.

6. L. Y. Zanette, A. F. White, M. C. Allen, and M. Clinchy, "Perceived Predation Risk Reduces the Number of Offspring Songbirds Produce Per Year," *Science* 334, no. 6061 (2011): 1398–1401, https://doi.org/10.1126/science.1210908.

7. M. Clinchy, M. J. Sheriff, and L. Y. Zanette, "Predator-Induced Stress and the Ecology of Fear," *Functional Ecology* 27, no. 1 (2013): 56–65, https://doi.org/10.1111/1365-2435.12007.

8. X. Wang, L. Zanette, and X. Zou, "Modelling the Fear Effect in Predator–Prey Interactions," *Journal of Mathematical Biology* 73, no. 5 (2016): 1179–1204, https://doi.org/10.1007/s00285-016-0989-1.

9. X. Wang and X. Zou, "Modeling the Fear Effect in Predator–Prey Interactions With Adaptive Avoidance of Predators," *Bulletin of Mathematical Biology* 79, no. 6 (2017): 1325–1359, https://doi.org/10.1007/s11538-017-0287-0.

10. S. K. Sasmal and Y. Takeuchi, "Dynamics of a Predator-Prey System With Fear and Group Defense," *Journal of Mathematical Analysis and Applications* 481, no. 1 (2020): 123471, https://doi.org/10.1016/j.jmaa.2019.123471.

11. P. Panday, N. Pal, S. Samanta, and J. Chattopadhyay, "Stability and Bifurcation Analysis of a Three-Species Food Chain Model With Fear," *International Journal of Bifurcation and Chaos* 28, no. 01 (2018): 1850009, https://doi.org/10.1142/s0218127418500098.

12. K. Sarkar and S. Khajanchi, "Impact of Fear Effect on the Growth of Prey in a Predator-Prey Interaction Model," *Ecological Complexity* 42 (2020): 100826, https://doi.org/10.1016/j.ecocom.2020.100826.

13. S. Mondal, A. Maiti, and G. P. Samanta, "Effects of Fear and Additional Food in a Delayed Predator–Prey Model," *Biophysical Reviews and Letters* 13, no. 04 (2018): 157–177, https://doi.org/10.1142/s1793048018500091.

14. E. L. Preisser and D. I. Bolnick, "The Many Faces of Fear: Comparing the Pathways and Impacts of Nonconsumptive Predator Effects on Prey Populations," *PLoS One* 3, no. 6 (2008): e2465, https://doi.org/10.1371/journal.pone.0002465.

15. R. Stoks, L. Govaert, K. Pauwels, B. Jansen, and L. De Meester, "Resurrecting Complexity: The Interplay of Plasticity and Rapid Evolution in the Multiple Trait Response to Strong Changes in Predation Pressure in the Water Flea Daphnia magna," *Ecology Letters* 19, no. 2 (2016): 180–190, https://doi.org/10.1111/ele.12551.

16. G. C. Trussell, P. J. Ewanchuk, and C. M. Matassa, "The Fear of Being Eaten Reduces Energy Transfer in a Simple Food Chain," *Ecology* 87, no. 12 (2006): 2979–2984, https://doi.org/10.1890/0012-9658(2006)87[2979:tfober]2.0.co;2.

17. D. E. Sadava, G. H. Orians, C. Heller, and W. K. Purves, *Life Study Guide: The Science of Biology* (Macmillan, 2006).

18. M. E. Clark, T. G. Wolcott, D. L. Wolcott, and A. H. Hines, "Intraspecific Interference Among Foraging Blue Crabs *Callinectes sapidus*: Interactive Effects of Predator Density and Prey Patch Distribution," *Marine Ecology Progress Series* 178 (1999): 69–78, https://doi.org/10.3354/meps178069.

19. M. Haque, "A Detailed Study of the Beddington–DeAngelis Predator–Prey Model," *Mathematical Biosciences* 234, no. 1 (2011): 1–16, https://doi.org/10.1016/j.mbs.2011.07.003.

20. R. Lande, "Risks of Population Extinction From Demographic and Environmental Stochasticity and Random Catastrophes," *The American Naturalist* 142, no. 6 (1993): 911–927, https://doi.org/10.1086/285580.

21. R. M. May, "Stability in Randomly Fluctuating Versus Deterministic Environments," *The American Naturalist* 107, no. 957 (1973): 621–650, https://doi.org/10.1086/282863.

22. P. J. Pal, S. Sarwardi, T. Saha, and P. K. Mandal, "Mean Square Stability in a Modified Leslie-Gower and Holling-Type Ii Predator-Prey Model," *Journal of Applied Mathematics and Informatics* (2011): 781–802.

23. Q. Wang and S. Zhang, "Dynamics of a Stochastic Delay Predator-Prey Model With Fear Effect and Diffusion for Prey," *Journal of Mathematical Analysis and Applications* 537, no. 2 (2024): 128267, https://doi.org/10.1016/j.jmaa.2024.128267.

24. Sajan, S. K. Sasmal, and B. Dubey, "A Phytoplankton–Zooplankton–Fish Model With Chaos Control: In the Presence of Fear Effect and an Additional Food," *Chaos: An Interdisciplinary Journal of Nonlinear Science* 32, no. 1 (2022): 013114, https://doi.org/10.1063/5.0069474.

25. A. A. Thirthar, S. J. Majeed, M. A. Alqudah, P. Panja, and T. Abdeljawad, "Fear Effect in a Predator-Prey Model With Additional Food, Prey Refuge and Harvesting on Super Predator," *Chaos, Solitons and Fractals* 159 (2022): 112091, https://doi.org/10.1016/j.chaos.2022.112091.

26. P. Panday, N. Pal, S. Samanta, P. Tryjanowski, and J. Chattopadhyay, "Dynamics of a Stage-Structured Predator-Prey Model: Cost and Benefit of Fear-Induced Group Defense," *Journal of Theoretical Biology* 528 (2021): 110846, https://doi.org/10.1016/j.jtbi.2021.110846.

27. A. I. Khibnik and B. Krauskopf, *Nonlinear Dynamics of Interacting Populations* (World Scientific Publishing Co, 1998).

28. A. Jana and A. Chatterjee, "Deterministic-Stochastic Analysis of a Two Species Predator-Prey System Under the Influence of Intraspecific Competition and Fear Effect," *Mathematical Methods in the Applied*

Sciences 48, no. 16 (2025): 14920–14940, https://doi.org/10.1002/mma.11223.

29. S. Wiggins, S. Wiggins, and M. Golubitsky, "Introduction to Applied Nonlinear Dynamical Systems and Chaos," *Spring* 2, no. 3 (New York, 2003).

30. A. Chatterjee, M. A. Abbasi, E. Venturino, J. Zhen, and M. Haque, "A Predator–Prey Model With Prey Refuge: Under a Stochastic and Deterministic Environment," *Nonlinear Dynamics* 112, no. 15 (2024): 13667–13693, https://doi.org/10.1007/s11071-024-09756-9.

31. R. I. Bogdanov, "Versal Deformations of a Singular Point of a Vector Field on the Plane in the Case of Zero Eigenvalues," *Functional Analysis and Its Applications* 9, no. 2 (1975): 144–145, https://doi.org/10.1007/bf01075453.

32. F. Takens, *Singularities of vector fields* (Publications Mathématiques de l'IHÉS, 1974).

33. S. N. Chow, C. Li, and D. Wang, *Normal Forms and Bifurcation of Planar Vector Fields* (Cambridge University Press, 1994).

34. P. K. Tapaswi and A. Mukhopadhyay, "Effects of Environmental Fluctuation on Plankton Allelopathy," *Journal of Mathematical Biology* 39, no. 1 (1999): 39–58, https://doi.org/10.1007/s002850050162.

35. E. Beretta, V. Kolmanovskii, and L. Shaikhet, "Stability of Epidemic Model With Time Delays Influenced by Stochastic Perturbations," *Mathematics and Computers in Simulation* 45, no. 3-4 (1998): 269–277, https://doi.org/10.1016/s0378-4754(97)00106-7.

36. I. I. Gikhman and A. V. Skorokhod, *The Theory of Stochastic Processes II* (Springer Science and Business Media, 2004).

37. A. Chatterjee and S. Pal, "The Influence of Fear on Intraspecific Competition in Predator-Prey Dynamics: A Model-Based Study," *Trends in Biomathematics: Exploring Epidemics, Eco-Epidemiological Systems, and Optimal Control Strategies: Selected Works From the BIOMAT Consortium Lectures* 2023 (Rio de Janeiro, Brazil, 2024): 33–66.

38. L. Shaikhet, *Lyapunov Functionals and Stability of Stochastic Functional Differential Equations* (Springer Science and Business Media, 2013).

39. V. N. Afanasiev, V. Kolmanovskii, and V. R. Nosov, *Mathematical Theory of Control Systems Design* (Springer Science & Business Media, 2013).

40. M. Bandyopadhyay and J. Chattopadhyay, "Ratio-Dependent Predator–Prey Model: Effect of Environmental Fluctuation and Stability," *Nonlinearity* 18, no. 2 (2005): 913–936, https://doi.org/10.1088/0951-7715/18/2/022.

41. D. Mukherjee, "Role of Fear in Predator–Prey System With Intraspecific Competition," *Mathematics and Computers in Simulation* 177 (2020): 263–275, https://doi.org/10.1016/j.matcom.2020.04.025.

42. A. Hastings, "Transients: The Key to Long-Term Ecological Understanding?" *Trends in Ecology and Evolution* 19, no. 1 (2004): 39–45, https://doi.org/10.1016/j.tree.2003.09.007.

43. L. J. Allen, *An Introduction to Stochastic Processes With Applications to Biology* (CRC Press, 2010).

44. S. P. Ellner and P. Turchin, "Chaos in a Noisy World: New Methods and Evidence From Time-Series Analysis," *The American Naturalist* 145, no. 3 (1995): 343–375, https://doi.org/10.1086/285744.

45. R. M. May, *Stability and Complexity in Model Ecosystems* (Princeton university press, 2001).

46. M. Scheffer, S. Carpenter, J. A. Foley, C. Folke, and B. Walker, "Catastrophic Shifts in Ecosystems," *Nature* 413, no. 6856 (2001): 591–596, https://doi.org/10.1038/35098000.

47. G. Birkhoff and G. C. Rota, in *Ordinary Differential Equation* (Stability and Complexity in Model Ecosystems, 1982).

48. T. C. Gard and T. G. Hallam, "Persistence in Food webs—I Lotka-Volterra Food Chains," *Bulletin of Mathematical Biology* 41, no. 6 (1979): 877–891, https://doi.org/10.1007/bf02462384.

49. M. Haque, M. S. Rahman, E. Venturino, and B. L. Li, "Effect of a Functional Response-Dependent Prey Refuge in a Predator–Prey Model," *Ecological Complexity* 20 (2014): 248–256, https://doi.org/10.1016/j.ecocom.2014.04.001.

50. M. S. Rahman, S. Pramanik, and E. Venturino, "An Ecoepidemic Model With Healthy Prey Herding and Infected Prey Drifting Away," *Nonlinear Analysis Modelling and Control* 28, no. 2 (2023): 1–39, https://doi.org/10.15388/namc.2023.28.31549.

Appendix A

Appendix A1: Proof of Proposition 1

The non-negativity of $x(t)$ and $y(t)$ follows from their exponential solution representations given by

$$\begin{aligned} x(t) &= x_0 \exp\left\{\int_0^t \left[\frac{r}{Ky(\hat{s})+1} - r_1 x(\hat{s}) - \frac{my(\hat{s})}{ax(\hat{s})+b}\right] d\hat{s}\right\}, \\ y(t) &= y_0 \exp\left\{\int_0^t \left[\frac{emx(\hat{s})}{ax(\hat{s})+b} - d - hy(\hat{s})\right] d\hat{s}\right\}, \end{aligned} \tag{A.1}$$

with $x_0, y_0 > 0$. Accordingly, $x(t)$ and $y(t)$ stay positive for every $t > 0$, which ensures that the interior of $\mathbb{R}^2_+$ remains invariant under the dynamics of System (1).

Appendix A2: Proof of Proposition 2

Let us consider the function

$$\widehat{W}(t) = x + \frac{1}{e}y. \tag{A.2}$$

The time derivative along a solution of (1) is

$$\frac{d\widehat{W}(t)}{dt} = x\left(\frac{r}{Ky+1} - r_1 x\right) - \frac{dy}{e} - \frac{hy^2}{e}. \tag{A.3}$$

For any $\gamma > 0$, the following estimate is satisfied:

$$\begin{aligned} \frac{d\widehat{W}}{dt} + \gamma\widehat{W} &\le x(r + \gamma - r_1 x) + \frac{\gamma - d}{e}y, \\ &\le \frac{(r+\gamma)^2}{4r_1} + \frac{\gamma - d}{e}y. \end{aligned} \tag{A.4}$$

We choose γ such that $\gamma < \min\{r, d\}$. Under this condition, inequality (A.4) reduces to

$$\frac{d\widehat{W}}{dt} + \gamma\widehat{W} \le \widehat{M}. \tag{A.5}$$

Applying the comparison theorem [47] yields

$$0 \le \widehat{W}(x(t), y(t)) \le \frac{\widehat{M}}{\gamma} + \widehat{W}(x(0), y(0))/e^{\gamma t}. \tag{A.6}$$

As $t \longrightarrow \infty$, $0 < \widehat{W}(t) \le \widehat{M}/\gamma$, which implies that System (1) is bounded.

Appendix A3: Proof of Proposition 3

We follow the approach of [37, 48] to demonstrate persistence by selecting a candidate Lyapunov function as $V_1(x, y) = x^{\widehat{\zeta}_1} y^{\widehat{\zeta}_2}$, where $\widehat{\zeta}_1$ and $\widehat{\zeta}_2$ are real constants. This choice yields the corresponding average Lyapunov derivative as follows:

$$\Gamma(x,y) = \frac{\dot{V}_1}{V_1} = \widehat{\zeta}_1 \frac{\dot{x}}{x} + \widehat{\zeta}_2 \frac{\dot{y}}{y}$$
$$= \widehat{\zeta}_1 \left(\frac{r}{Ky+1} - r_1 x - \frac{my}{ax+b} \right) \tag{A.7}$$
$$+ \widehat{\zeta}_2 \left(\frac{emx}{ax+b} - d - hy \right).$$

It remains to verify that the function is positive at each boundary equilibrium. At E_0, we compute $\Gamma(0,0) = \widehat{\zeta}_1 r - \widehat{\zeta}_2 d$. By taking $\widehat{\zeta}_1 = \widehat{\zeta}_2 = \widehat{\zeta}$, this expression reduces to $\Gamma(0,0) = \widehat{\zeta}(r-d)$. Under Condition (7), we have $\widehat{\zeta}(r-d) > 0$, which guarantees positivity at the trivial equilibrium E_0.

At the predator-free equilibrium E_1, the function Γ attains the form

$$\Gamma\left(\frac{r}{r_1}, 0\right) = \widehat{\zeta}\left(\frac{emr}{ar + br_1} - d \right) > 0. \tag{A.8}$$

Condition (8) ensures that this criterion is satisfied. Consequently, the positivity of $\Gamma(x,y)$ at each boundary equilibrium establishes the persistence of System (1). Moreover, due to its uniform persistence, there exist positive constants $\widehat{\rho}_1$ and t_1 such that $\forall t > t_1$, and the conditions $x(t) > \widehat{\rho}_1$ and $y(t) > \widehat{\rho}_1$ are satisfied.

Appendix A4: Proof of Proposition 4

The Lyapunov function defined in (4.3) works for System (1). Let us rename it as

$$\widehat{V}(x,y) = x - x^* - x^* \ln \frac{x}{x^*} + \frac{b + ax^*}{be} \left(y - y^* - y^* \ln \frac{y}{y^*} \right). \tag{A.9}$$

The first-order derivative of $\widehat{V}$ is

$$\begin{aligned}
\frac{d\widehat{V}}{dt} &= \frac{\partial \widehat{V}}{\partial x}\frac{dx}{dt} + \frac{\partial \widehat{V}}{\partial y}\frac{dy}{dt} \\
&= \left(1 - \frac{x^*}{x}\right)\left[rx - r_1 x^2 - \frac{mxy}{ax+b} \right] + \frac{b+ax^*}{be}\left(1 - \frac{y^*}{y}\right)\left[\frac{emxy}{ax+b} - dy - hy^2 \right] \\
&= (x - x^*)\left[r - r_1 x - \frac{my}{ax+b} - \left(r - r_1 x^* - \frac{my^*}{ax+b} \right) \right] \\
&\quad + \frac{b+ax^*}{be}(y - y^*)\left[\frac{emy}{ax+b} - d - hy - \left(\frac{emy^*}{ax^*+b} - d - hy^* \right) \right] \\
&= (x - x^*)\left[-r_1(x - x^*) - \frac{mb(y - y^*)}{(ax+b)(ax^*+b)} \right. \\
&\quad \left. - \frac{am\{x^*(y - y^*) - y^*(x - x^*)\}}{(ax+b)(ax^*+b)} \right] + \frac{b+ax^*}{be}(y - y^*)\left[\frac{ebm(x - x^*)}{(ax+b)(ax^*+b)} - h(y - y^*) \right] \\
&\leq -\left[r_1 - \frac{amy^*}{ax^*+b} \right](x - x^*)^2 - \frac{h(b+ax^*)}{be}(y - y^*)^2.
\end{aligned} \tag{A.10}$$

Therefore, we obtain $(d\widehat{V})/(dt) < 0$ if $r_1 > (amy^*)/(ax^* + b)$. Moreover, $(d\widehat{V})/(dt) = 0$ only if $x = x^*$, and $y = y^*$. As per LaSalle's invariance principle, $E^*(x^*, y^*)$ is globally asymptotically stable.

Appendix A5: Proof of Proposition 5

Setting the trace of the Jacobian matrix equal to zero yields

$$m = \left[\frac{hy^*}{x^*} + r_1 \right] \frac{(ax^* + b)^2}{ay^*} = m^H. \tag{A.11}$$

The condition $[\det(J^*)]_{m=m^H} > 0$ is equivalent to stating that the characteristic equation $\lambda^2 + [\det(J^*)]_{m=m^H} = 0$ has roots that are purely imaginary.

For $m = m^H$, the characteristic equation of the system reduces to

$$\chi^2 + \widehat{\omega} = 0, \quad \widehat{\omega} = [\det(J^*)]_{m=m^H} > 0. \tag{A.12}$$

Hence, Equation (A.12) possesses two roots: $\chi_1 = +i\sqrt{\widehat{\omega}}$ and $\chi_2 = -i\sqrt{\widehat{\omega}}$. For values of m near m^H, the eigenvalues of J^* take the form $\chi_{1,2} = \widehat{\lambda}_1(m) + \pm i\widehat{\lambda}_2(m)$, where

$$\widehat{\lambda}_1(m) = \frac{tr(J^*)}{2},$$
$$\widehat{\lambda}_2(m) = \sqrt{\det(J^*) - \frac{tr(J^*)}{4}}. \tag{A.13}$$

The transversality condition needs to be confirmed, which states that

$$\frac{d}{dm}\left(\mathrm{Re}(\chi_j(m))\right)_{m=m^H} \neq 0, \quad j = 1, 2. \tag{A.14}$$

By substituting $\chi_1 = \widehat{\lambda}_1(m) + i\widehat{\lambda}_2(m)$ into Equation (A.12) and taking the derivative with respect to m, we derive

$$\begin{aligned}
2\widehat{\lambda}_1(m)\widehat{\lambda}_1'(m) - 2\widehat{\lambda}_2(m)\widehat{\lambda}_2'(m) + \widehat{\omega}' &= 0, \\
2\widehat{\lambda}_2(m)\widehat{\lambda}_1'(m) + 2\widehat{\lambda}_1(m)\widehat{\lambda}_2'(m) &= 0.
\end{aligned} \tag{A.15}$$

Solving (A.15), we get

$$\frac{d}{dm}\left(\mathrm{Re}(\chi_j(m))\right)_{m=m^H} = \frac{-2\widehat{\lambda}_1\widehat{\omega}'}{2\left(\widehat{\lambda}_1^2 + \widehat{\lambda}_2^2\right)} \neq 0; \tag{A.16}$$

i.e.,

$$\frac{d}{dm}[tr(J^*)]_{m=m^H} \neq 0, \tag{A.17}$$

which guarantees that the transversality requirement holds. The bifurcation results further indicate that elevated per capita predation rates may induce oscillatory dynamics, potentially leading both populations to exhibit sustained fluctuations.

Appendix A6: Proof of Proposition 7

At $m = m^{TC}$, the Jacobian matrix J_1 corresponding to System (1) at E_1 admits a simple zero eigenvalue. Let U_1 and V_1 denote the right and left eigenvectors associated with the zero eigenvalue of J_1 and its transpose $(J_1)^T$, respectively. A straightforward computation yields

$$U_1 = \begin{pmatrix} -\frac{J_{12}^{E_1}}{J_{11}^{E_1}} 1 \end{pmatrix}^T$$
$$V_1 = (01)^T. \tag{A.18}$$

We have then

$$F_m(x, y) = \begin{pmatrix} -\frac{xy}{ax+b} & \frac{exy}{ax+b} \end{pmatrix}^T,$$
$$F_m\left(E_1; m = m^{TC}\right) = \begin{pmatrix} 0 & 0 \end{pmatrix}^T, \tag{A.19}$$
$$(V_1)^T F_m\left(E_1; m = m^{TC}\right) = 0.$$

Also, $DF_m(E_1; m = m^{TC})U_1 = (-(x_1/(ax_1 + b))(ex_1)/(ax_1 + b))^T$. We, therefore, obtain

$$(V_1)^T\left[DF_m\left(E_1; m = m^{TC}\right)(U_1)\right] = \frac{ex_1}{ax_1 + b} \neq 0. \tag{A.20}$$

Further,

$$(V_1)^T D^2 F\left(E_1; m = m^{TC}\right)(U_1, U_1) = -\frac{2beJ_{12}^{E_1}}{J_{11}^{E_1}(ax_1 + b)^2} \neq 0. \tag{A.21}$$

Application of Sotomayor's theorem [37, 49, 50] confirms that a TCB is generated at E_1 as m passes through the critical value m^{TC}.

Appendix A7: Proof of Proposition 6

Let us denote the Lyapunov function as

$$\Theta(u(t)) = \frac{1}{2}\left[u_1^2 + \omega_1 u_2^2\right], \tag{A.22}$$

where real positive constants ω_1 will be determined subsequently. It is easy to confirm that inequalities (52) hold true when $\gamma = 2$. Moreover,

$$L_\Theta(u(t)) = \left(-\widehat{a}_{11}u_1 - \widehat{a}_{12}u_2\right)u_1 - \widehat{a}_{12}u_2)u_1 + \left(\widehat{a}_{21}u_1 - \widehat{a}_{22}u_2\right)\omega_1 u_2$$
$$+ \frac{1}{2}\mathrm{tr}\left[g^T(u(t))\frac{\partial^2\Theta}{\partial u^2}g(u(t))\right]. \tag{A.23}$$

Now, we assess that

$$\frac{\partial^2\Theta}{\partial u^2} = \begin{bmatrix} 1 & 0 \\ 0 & \omega_1 \end{bmatrix}, \tag{A.24}$$

and $g^T(u(t))((\partial^2\Theta)/(\partial u^2))g(u(t)) = \begin{bmatrix} \sigma_1^2 u_1^2 & 0 \\ 0 & \omega_1\sigma_2^2 u_2^2 \end{bmatrix}$. This allows the trace term to be evaluated as follows:

$$\mathrm{tr}\left[g^T(u(t))\frac{\partial^2\Theta}{\partial u^2}g(u(t))\right] = \sigma_1^2 {u_1}^2 + \omega_1\sigma^2 {u_2}^2. \tag{A.25}$$

Hence, from (A.25), we obtain $L_\Theta(u(t)) = -(\widehat{a}_{11} - \sigma_1^2/2)u_1^2 - (\widehat{a}_{12} - \widehat{a}_{21}\omega_1)u_1u_2 - (\widehat{a}_{22} - \sigma_2^2/2)\omega_1 u_2^2$. By selecting $\omega_1 = \widehat{a}_{12}/\widehat{a}_{21}$, we derive the following form of $L_\Theta(u(t))$:

$$L_\Theta(u(t)) = -\left(\widehat{a}_{11} - \frac{\sigma_1^2}{2}\right)u_1^2 - \left(\widehat{a}_{22} - \frac{\sigma_2^2}{2}\right)\omega_1 u_2^2 = -u^T Q u. \tag{A.26}$$

Defining $Q = \mathrm{diag}[(\widehat{a}_{11} - \sigma_1^2/2), (\widehat{a}_{22} - \sigma_2^2/2)\omega_1]$, we note that Q is a real symmetric positive definite matrix. Consequently, its eigenvalues λ_1 and λ_2 are positive real values iff the following condition: $\sigma_1^2 < 2\widehat{a}_{11}$ with $\widehat{a}_{11} > 0$ and $\sigma_2^2 < 2\widehat{a}_{22}$ holds. Let $\lambda_m = \min\{\lambda_1, \lambda_2\}$, where λ_1 and λ_2 are the positive eigenvalues of the associated diagonal matrix. Then, the preceding estimate for $L_\Theta(u(t))$ implies

$$L_\Theta(u(t)) \leq -\lambda_m|u(t)|^2. \tag{A.27}$$

Hence, the proof is established.